AIChE

Performance Analysis of a New Hybrid Cooling–Drying System

Merve Senturk Acar[a] and Oguz Arslan [b]

[a]Tavsanlı Vocational School, Dumlupinar University, Kutahya 43300, Turkey; merve.senturkacar@dpu.edu.tr (for correspondence)
[b]Mechanical Engineering Department, Engineering Faculty, Bilecik Seyh Edebali University, Bilecik 11230, Turkey; oguz.arslan@bilecik.edu.tr (for correspondence)

Published online 27 November 2017 in Wiley Online Library (wileyonlinelibrary.com). DOI 10.1002/ep.12832

In this study, the Ranque–Hilsch vortex tube (RHVT)-aided hybrid cooling and drying system (RHVTHCD), nonhybrid cooling and drying system (NCDS), and RHVT-aided hybrid cooling and drying system in which used the input stream of RHVT is obtained from the different system as a waste (RHVTHCDW) were investigated using energy and exergy analysis. In this aim, many systems were designed and evaluated with net present value (NPV) in the viewpoint of life cycle cost (LCC). Additionally, several RHVTs with the 9 different helical vortex generators, 3 different control valve angle ($\alpha = 30°$, 45°, and 60°), 3 different vortex tube body (480, 350, and 210 mm), 5 different opening position of the control valve, and 5 different inlet flow pressure of RHVT (201.325–601.325 kPa) were performed experimentally. The cold outlet flow of RHVT was integrated to the vapor compression system with a heat exchanger, where the hot one was integrated in the drying system. The energy and exergy efficiencies of RHVTHCD system increase with the increase of the evaporator temperature. The maximum NPV value of the RHVTHCD system obtained was 37256.63 €. The highest energy and exergy efficiencies were calculated as 24.74% and 9.69%, respectively. © 2017 American Institute of Chemical Engineers Environ Prog, 37: 1808–1828, 2018

Keywords: economic analysis, energy analysis, exergy analysis, hybrid of cooling and drying, vortex tube

INTRODUCTION

As a result of the rapid increase of the population, the sustainability of the food supply and energy sources have gained importance. The drying and cooling are regional methods used for long-term storage of foods for decades. Sun drying is cheaper than other drying methods, but the length of drying time, the low quality of the final product, and dependence on weather conditions were disadvantages of the sun drying [1]. These negative factors cause began to be used the artificial mechanical drying methods. However, these methods make the energy requirements increase. Because of the limited energy resources and increasing energy needs will require the use of energy efficient. For the recent years, the studies, aiming to improve the energy and exergy efficiency of the drying and cooling systems have much more importance [2–4].

The vortex tube was discovered by Ranque in 1933 [5]. Ranque–Hilsch vortex tube (RHVT) consists of a principal tube, which a high-pressure gas stream enters tangentially and the high-pressure gas pass through the helical generator and then a swirling flow occurred in the RHVT body which resulted in the hot and cold streams were separated [5–7]. In literature, the hot and cold streams of RHVT were analyzed by energy and exergy analysis [8,9]. Sommers and Jacobi studied to improve the heat transfer on the air side of the cooling evaporator used with vortex generator [10]. Aydın and Baki investigated the design parameters and performances of counterflow vortex tubes experimentally [11]. Dincer and Baskaya (2009) examined the change of exergy efficiency of the Ranque–Hilsch vortex tube for the five different values of the control valve angle ($\alpha = 30°$, 60°, 90°, 120°, and 150°) and the different values of the pressure of the inlet flow [12]. Maximum exergy was achieved at $\alpha = 90°$ and inlet flow pressure of 320 kPa. Kabeel et al. (2010) were theoretically and experimentally investigated the cooling performance of a tractor cabinet by using RHVT [13]. They have determined that the temperature of the feed air must be reduced or the velocity increased in order to improve the spot cooling performance. Saidi and Vaalipour (2003) investigated the effects diameter and body length of the RHVT, and nozzle number of RHVT generator on the cold temperature difference in a counter-flow vortex tube [6]. They have determined the maximum cold air temperature difference was found for RHVT body length to tube diameter ratio ranged from 20 to 55.5. Rafiee and Sadeghiazad [14] were investigated the heat transfer and energy separation inside a counter-flow vortex tube for different shapes of hot control valves. Kumar et al. [15] were experimentally investigated the cold/hot temperature and humidity separations in vortex tube for the different fractions of the cold mass at the different pressures. Cebeci et al. [16] investigated the effects of the orifice nozzle number and the inlet pressure on heating and cooling performance of a counterflow Ranque–Hilsch type vortex tube. Dutta et al. [17], Thakare, and Parekh [18,19] investigated the energy separation phenomena using computational fluid dynamics (CFD) model for RHVT.

The usage of RHVT is one of the methods to improve the coefficient of performance (*COP*) and exergy efficiency of the vapor compression cooling system. As first, Hooper and Ambrose (1973) used RHVT in the refrigeration system as a throttling valve and tested the system for 13 different refrigerants [20]. Then, many studies were conducted for the direct use of RHVT in the cooling system taking the different geometries of RHVT, the different operating parameters, the

different refrigerants and the different system configurations [21–23]. Acar and Arslan (2016) were theoretically and experimentally investigated the NPV, energy, and exergy efficiency of drying system by using RHVT [24].

The studies in the literature are focused on the cold outlet flow of RHVT, the energy and exergy analysis of RHVT and the temperature differences between outlet streams. In addition, the NPV values of these systems are not considered in these studies. There is no study about the availability of the outlet flows of RHVT in any hybrid system. In this study, the RHVT aided hybrid cooling and drying system (RHVTHCD) was investigated by the energy, exergy analysis and evaluated with net present value (NPV) in the viewpoint of life cycle cost (LCC). In this system, it is aimed to increase the energy and exergy efficiencies of the cooling and drying system which was integrated with RHVT outlet flows. The hot outlet flow of RHVT integrated to the drying system before the electrical heater and the cold outlet flow of RHVT was used in the vapor compression cycle. The RHVT experiments were performed for 9 different helical vortex generators, 3 different control valve angel ($\alpha = 30°$, 45°, and 60°), 3 different vortex tube body(480, 350, and 210 mm), 5 different opening position of the control valve and 5 different pressures of the inlet flow of RHVT (201.325–601.325 kPa). The experimental results of the RHVT were used to design of the hybrid system. The inlet temperatures of dryer (328.15, 333.15, 338.15, and 343.15 K), outlet temperatures of dryer, the compressor outlet pressure of refrigerant (1300, 1700, and 2000 kPa), the evaporator temperature (275.15, 276.15, and 277.15 K), 4 different refrigerants (R-134a, R-143a, R-404a, and R-507a), and the cold mass fraction were taken into account for the RHVTHCD system designs. The NPV, energy, and exergy efficiency values were calculated for three different cooling and drying system. The first one of these systems is the Ranque–Hilsch vortex tube aided cooling and drying system named as a hybrid system. The second one is also a hybrid system; however, the compressed air is obtained as a waste from an external source (RHVTHCDW). And the last one is considered as the conventional system named the nonhybrid cooling and drying system (NCDS).

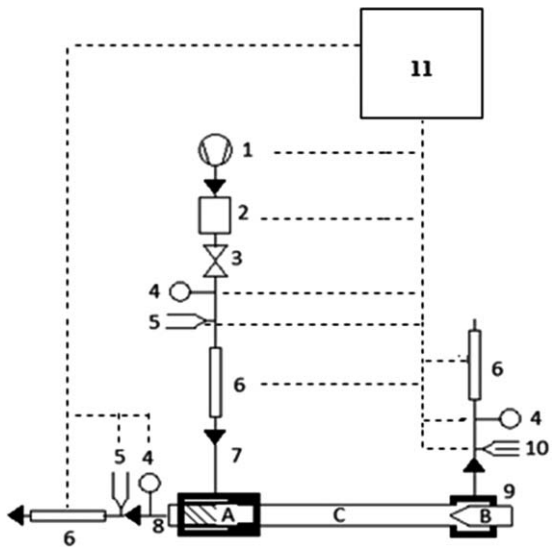

Figure 1. The schematic of the experimental set-up of RHVT.

EXPERIMENTAL SET-UP OF RHVT

The schematic diagram of experimental set-up of RHVT was given in Figure 1. The air was compressed by a pressure-adjustable air-cooled compressor (1). The compressed air was stored in pressure tank (2) (a capacity of 0.3 m^3). The volumetric rate of the compressed air was adjusted by means of a spherical valve (3). The compressed air enters to the helical vortex generator (A) and then the swirling flow occurs in the RHVT body (C). This flow is separated into hot and cold streams in RHVT body by means of the control valve (B).

The pressure and volumetric rate of the cold and inlet streams were measured by a relative pressure transmitter (4) and an air flowmeter (6). The volumetric rate of the hot side was calculated using the conservation law of mass. The temperature of the cold stream and compressed inlet air were measured by a PT100 type of thermocouple (5). The temperature of the hot stream was measured by a relative humidity and temperature transmitter (10). All the measured data was then stored in a data logger (11). The energy consumption of compressor was also measured and stored by a network analyzer integrated to the data logger. The technical properties of the measurement devices were given in Table 1 [24,25].

RHVT mainly consists of three components named as the helical vortex generator, control valve and RHVT body (Figure 2). The used geometrical parameters of RHVT were chosen as height (b), width (w) of the channel, inner diameter (d) of the helical vortex generators, and length (L) and diameter (D) of RHVT bodies. All the helical vortex generators have a single nozzle and 3 different control valve angles were used ($\alpha = 30°$, 45°, and 60°) in RHVT. The technical properties of RHVT used in experiments were given in Table 2 [24,25].

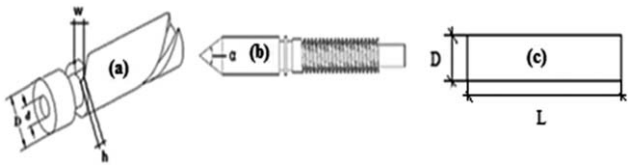

Figure 2. The helical vortex generator (a), control valve (b), and RHVT body (c).

Table 1. Technical properties of the measurement devices [24,25].

Device	Type	Property	Sensibility
Thermocouple	Testo, PT 100	223.15–573.15 K	±0.05 K
Relative pressure transmitter	WİKA S-10	0–1000 kPa	±0.5% kPa
Flow meter (cold stream)	Testo 6441	0.25–75 $m^3\ h^{-1}$	±3% $m^3\ h^{-1}$
Flow meter (inlet stream)	Testo 6442	0.75–225 $m^3\ h^{-1}$	±0.3% $m^3\ h^{-1}$
Relative humidity and temperature transmitter	Testo 6881	233.15–453.15 K; 0–100% RH	±0.2 K; ±1% RH
Data logger	Elimko PR-100	12 channel, 85–265 VAC	-

Table 2. Technical properties of RHVT [24,25].

Property	*b* (mm)	*w* (mm)	*d* (mm)	*D* (mm)	*L* (mm)	*D* (mm)	*L*/*D*	α (°)
				Vortex generator				
0	2.0	4.5	6.15	12	-	-	-	-
A			3.3		-	-	-	-
B			5.1		-	-	-	-
C			6.0		-	-	-	-
D			7.1		-	-	-	-
M	1.5	6.0	3.3		-	-	-	-
N			5.1		-	-	-	-
O			5.7		-	-	-	-
J			7.1		-	-	-	-
				RHVT body				
1	-	-	-	-	480	12	40	-
2	-	-	-	-	350		29.17	-
3	-	-	-	-	210		17.5	-
				Control valve				
1	-	-	-	-	-	-	-	30
2	-	-	-	-	-	-	-	45
3	-	-	-	-	-	-	-	60

Table 3. The uncertainties of the measurements [24,25].

Measurement devices	Uncertainty (*U*)
Thermocouple (T_6)	±0.264 K
Thermocouple (T_8)	±0.445 K
Relative pressure transmitter (P_8)	±5.68 kPa
Flowmeter (cold exit)	±0.218 $m^3\ h^{-1}$
Flowmeter (inlet stream)	±0.303 $m^3\ h^{-1}$
Relative humidity and temperature transmitter (T_9, ϕ_9)	±0.490 K, ±0.154 RH

UNCERTAINTY ANALYSIS OF THE EXPERIMENTS

The measurements were evaluated with the uncertainty analysis. The average of the measurement ($\bar{X}$) is

$$\bar{X}=\frac{\sum X_m}{n} \tag{1}$$

where n is the number of the measurements and X_m is the measurement. Standard deviation (SD) is

$$\mathrm{SD}=\sqrt{\frac{\sum_{m=1}^{n}(X_m-\bar{X})^2}{(n-1)}} \tag{2}$$

Uncertainty (U) was given in Eq. (3) [26].

$$U=\frac{\mathrm{SD}}{\sqrt{n}} \tag{3}$$

The cold and hot streams pressures were accepted as 101.325 kPa as these streams outlet to the ambient. Therefore, the uncertainties of the pressure meters after cold and hot streams were not calculated. The uncertainties of the measurements were given in Table 3. According to the findings of the uncertainty analysis, it was determined that the obtained results of the measurements were acceptable for the use in the design of the RHVTVCC.

RHVT AIDED HYBRID COOLING AND DRYING SYSTEM (RHVTHCD)

RHVTHCD flow diagram is shown in Figure 3. The cold stream of RHVT was integrated into the refrigeration cycle with a heat exchanger after the evaporator. The refrigerant enters to the compressor at point 1 and the compressed refrigerant leaves at point 2. The condensed refrigerant enters to the heat exchanger at point 3 and gives the heat to the cold stream of RHVT. The refrigerant leaves the heat exchanger at point 4a and the cold stream of RHVT exits at point 7. The cold stream works as a cooling fluid. The refrigerant pressure is decreased to the inlet pressure of the compressor at the exit of the throttling valve (5). The ambient air is compressed then inlets to RHVT (8). The hot exit of RHVT (9) was integrated into the drying system before the electrical heater. The heated drying air (10) inlets to the dryer and takes the moisture of the fresh tomatoes and then leaves the dryer (11). The fresh tomatoes enter to the dryer at point 12 and the dried tomatoes leave the dryer at point 13.

The vapor compression cooling systems were designed for different compressor discharge pressure and suitable evaporator temperatures of cooling tomatoes. The compressor (C1) outlet pressure was chosen between 1300 and 2000 kPa. The pressure of the inlet stream of RHVT was changed between 201.325 and 601.325 kPa. The thermodynamic properties of refrigerant were determined by REFPROP. The parameters for designing of vapor compression cooling system handled in the study were given in Table 4 [25]. The thermodynamic properties of the RHVT inlet and outlet flows were determined using experimental results.

The Page model best described the drying curve of tomatoes [27]. So that, the temperatures of the inlet stream of the dryer, and drying periods were determined by using Page drying model for tomato. The variation of the drying period of tomato versus the temperature of the inlet stream of the dryer was given in Figure 4 [27]. The temperature differences of inlet and outlet stream of the dryer were adopted as 2, 5, 10, 15, and 20 K.

According to Figure 4, the drying period decreases with increasing the inlet stream temperature of the dryer. The tomato was reached the final moisture content level of 11% at the inlet stream temperature of the dryer as 328.15, 333.15, 338.15, and 348.15 K while the drying period of the tomato took 127,800, 100,800, 95,400, and 86,400 seconds, respectively [27]. The temperatures of the inlet and outlet streams of the dryer and the temperature of the fresh and dried product and drying periods were given in Table 5.

The temperature of the hot stream of RHVT was heated to the temperature of the inlet stream of the dryer using the

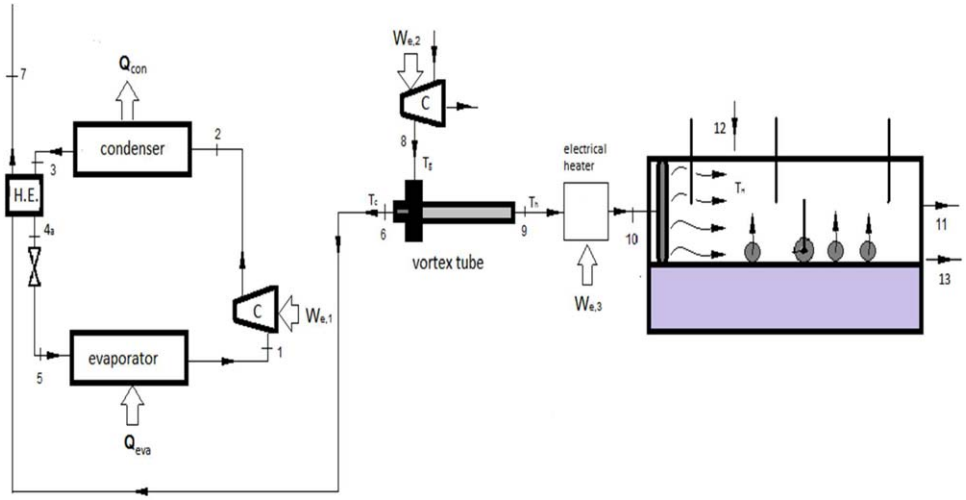

Figure 3. The flow diagram of the RHVTHCD. [Color figure can be viewed at **wileyonlinelibrary.com**]

Table 4. The design parameters for RHVTHCD system [25].

Evaporator temperature (T_1)	275.15–276.15–277.15 K
Refrigerants	R134a, R143a, R404a, R507a
Compressor exit pressure of the cooling system (P_2)	1300–2000 kPa

electrical heater. The efficiency of the electrical heater was determined with the experiments. The electrical wiring diagram of the electrical heater is shown in Figure 5 [25].

As seen in Figure 5, 13 (500 W) heater resistances are being used in the experiments. Here, 4 heater resistances connected in series (in three single lines) and one heater resistance connected to each other line in parallel. The schematic diagram and image of the experimental set-up of the electrical heater are given in Figure 6 [25].

The air compressed in the compressor (1) and collected in the air pressure tank (2). The flow of the air was setting by a spherical valve (3). The pressure, temperature, and flow of the air were measured with a relative pressure transmitter (4), thermocouple (5) and flowmeter (6), respectively. After the measurements, the compressed air enters to the electrical heater (7). The temperature and relative humidity of the heated air (8) were measured with relative humidity and temperature transmitter at point 9. The consumed power of electrical heater was measured. The electrical heater efficiency was calculated with Eq. (4).

$$\eta_{\mathrm{eh,exp}}=\frac{\dot{m}_{\mathrm{a}}\cdot c_{\mathrm{p,a}}\cdot\left(T_{\mathrm{he,out}}-T_{\mathrm{he,in}}\right)}{\dot{W}_{\mathrm{exp}}} \tag{4}$$

where $\dot{m}_{\mathrm{a}}$ is the air mass flow rate during the test (kg/s), $c_{\mathrm{p,a}}$ is the specific heat of air (kJ/kg·K), $\dot{W}_{\mathrm{exp}}$ is the consumed electric energy per unit of time (kW), $T_{\mathrm{eh,in}}$ is the temperature of the inlet air in electrical heater (K), and $T_{\mathrm{eh,out}}$ is the temperature of the outlet air of electrical heater (K). The experimental results of the electrical heater are as presented in Figure 7.

As seen in Figure 7, the mean value of the electrical heater efficiency is determined as 0.27 [25]. The inlet air temperature was included in the calculations as equal to the ambient temperature while the power consumption of electrical heater calculated for thermodynamic analysis of the electrical drying system.

Energy and Exergy Analysis

The following assumptions were handled in the energy analysis:

1. Potential and kinetic energy effects are negligible.
2. The compressor has an electrical (η_{e}) and mechanical efficiencies (η_{mec}) of 90%.
3. The compressor has an isentropic efficiency of 70%.
4. The heat exchanger has an efficiency of 70%.
5. The electrical heater has an electrical efficiency ($\eta_{\mathrm{e,h}}$) of 27%.
6. The RHTV outlet stream pressure equals to environment pressure (101.325 kPa).
7. The reference state is 101.325 kPa and 293.15 K.

Under these assumptions, the governing energy equations of the RHVTCT were obtained as follows.

Evaporator:

$$\dot{Q}_{\mathrm{eva}}=\dot{m}_{\mathrm{R}}\cdot(h_1-h_{4\mathrm{a}}) \tag{5}$$

Condenser:

$$\dot{Q}_{\mathrm{con}}=\dot{m}_{\mathrm{R}}\cdot(h_3-h_2) \tag{6}$$

Heat exchanger:

$$\dot{m}_6\cdot(h_7-h_6)=\dot{m}_{\mathrm{R}}\cdot(h_3-h_{4\mathrm{a}})+\dot{Q}_{\mathrm{he}} \tag{7}$$

Compressor 1 (vapor compression cooling system):

$$\dot{W}_1=\dot{m}_{\mathrm{R}}\cdot(h_2-h_1) \tag{8}$$

And electrical power of Compressor 1:

$$\dot{W}_{\mathrm{e,1}}=\frac{\dot{W}_1}{\eta_{\mathrm{mec}}\cdot\eta_{\mathrm{el}}} \tag{9}$$

Compressor 2 (RHVT):

$$\dot{W}_2=R\cdot T\cdot\ln\frac{P_{1,\mathrm{a}}}{P_8}\cdot\dot{m}_8 \tag{10}$$

And electrical power of Compressor 2:

$$\dot{W}_{e,2}=\frac{\dot{W}_2}{\eta_{\mathrm{mec}}\cdot\eta_{\mathrm{e}}} \tag{11}$$

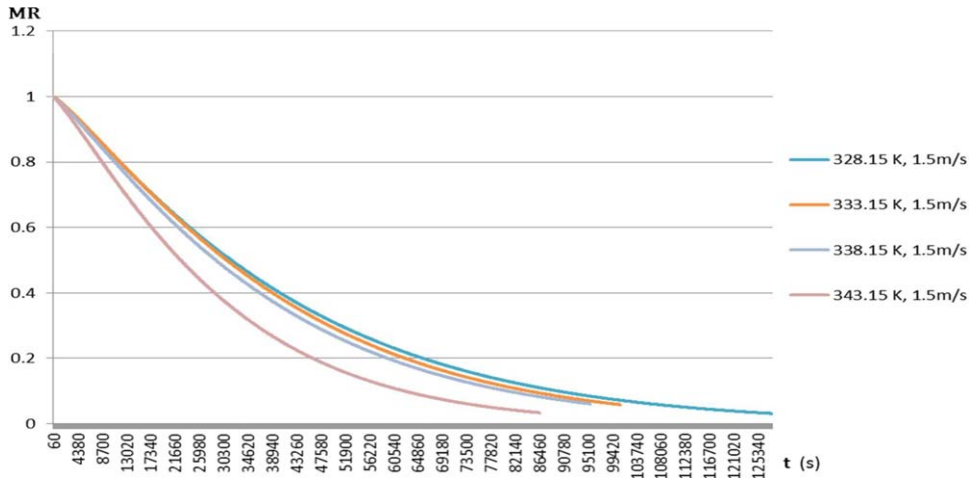

Figure 4. The variation of the drying period of tomato versus the temperature of the inlet stream of dryer [27]. [Color figure can be viewed at **wileyonlinelibrary.com**]

Table 5. The operating parameters of the dryer.

Drying period (s)	T_{10} (K)	T_{11} (K)	T_{12} (K)	T_{13} (K)
127,800	328.15	326.15	293.15	326.15
		323.15		323.15
		318.15		318.15
		313.15		313.15
		308.15		308.15
100,800	333.15	331.15		331.15
		328.15		328.15
		323.15		323.15
		318.15		318.15
		313.15		313.15
95,400	338.15	336.15		336.15
		333.15		333.15
		328.15		328.15
		323.15		323.15
		318.15		318.15
86,400	343.15	341.15		341.15
		338.15		338.15
		333.15		333.15
		328.15		328.15
		323.15		323.15

RHVT:

$$\dot{Q}_{\mathrm{RHVT}}=\dot{m}_6\cdot h_6+\dot{m}_9\cdot h_9-\dot{m}_8\cdot h_8 \tag{12}$$

Throttling valve:

$$\dot{m}_{\mathrm{R}}\cdot h_3=\dot{m}_{\mathrm{ref}}\cdot h_4 \tag{13}$$

Electrical heater:

$$\dot{W}_3=\dot{m}_9\cdot(h_{10}-h_9) \tag{14}$$

And electrical power of electrical heater:

$$\dot{W}_{\mathrm{e},3}=\frac{\dot{W}_3}{\eta_{\mathrm{eh}}} \tag{15}$$

Dryer:

$$\dot{m}_{10}\cdot(h_{10}-h_{11})=\dot{m}_{12}\cdot c_{\mathrm{p},12}\cdot(T_{13}-T_{12})+(\dot{m}_{12}-\dot{m}_{13})\cdot h_{\mathrm{db},13} \tag{16}$$

here, $c_{\mathrm{p},12}$: specific heat of tomato. The specific heat ($c_{\mathrm{p,tom}}$) of tomato, calculated with Eq. (17) depending on temperature and constituents of tomato [28]:

$$c_{\mathrm{p,tom}}=c_{\mathrm{pro}}X_{\mathrm{pro}}+c_{\mathrm{fat}}X_{\mathrm{fat}}+c_{\mathrm{car}}X_{\mathrm{car}}+c_{\mathrm{fib}}X_{\mathrm{fib}}+c_{\mathrm{ash}}X_{\mathrm{ash}}+c_{\mathrm{w}}X_{\mathrm{w}} \tag{17}$$

where X is the mass ratio of the food component. The mass composition ranges of tomato were given in Table 6.

The specific heat of the constituents of the product depending on temperature [28];

$$c_{\mathrm{pro}}=2.0082+1.2089\times10^{-3}\cdot T-1.3129\times10^{-6}\cdot T^2 \tag{18}$$

$$c_{\mathrm{fat}}=1.9842+1.4733\times10^{-3}\cdot T-4.8008\times10^{-6}\cdot T^2 \tag{19}$$

$$c_{\mathrm{car}}=1.5488+1.9625\times10^{-3}\cdot T-5.9399\times10^{-6}\cdot T^2 \tag{20}$$

$$c_{\mathrm{fiber}}=1.8459+1.8306\times10^{-3}\cdot T-4.6509\times10^{-6}\cdot T^2 \tag{21}$$

$$c_{\mathrm{ash}}=1.0926+1.8896\times10^{-3}\cdot T-3.6817\times10^{-6}\cdot T^2 \tag{22}$$

$$c_{\mathrm{w}}=4.1289-9.0864\times10^{-5}\cdot T+5.4731\times10^{-6}\cdot T^2 \tag{23}$$

Energy efficiency of RHVTHCD system:

$$\eta_1=\frac{\dot{Q}_{\mathrm{eva}}+\dot{m}_{10}\cdot(h_{10}-h_{11})}{\dot{W}_{\mathrm{e},1}+\dot{W}_{\mathrm{e},2}+\dot{W}_{\mathrm{e},3}+\dot{m}_8\cdot h_{1,\mathrm{a}}+\dot{Q}_{\mathrm{RHVT}}+\dot{Q}_{\mathrm{he}}+\dot{m}_{12}\cdot c_{\mathrm{p},12}\cdot T_{12}} \tag{24}$$

Energy efficiency of RHVTHCDW system:

$$\eta_2=\frac{\dot{Q}_{\mathrm{eva}}+\dot{m}_{10}\cdot(h_{10}-h_{11})}{\dot{W}_{\mathrm{e},1}+\dot{W}_{\mathrm{e},3}+\dot{m}_8\cdot h_8+\dot{Q}_{\mathrm{RHVT}}+\dot{Q}_{\mathrm{he}}+\dot{m}_{12}\cdot c_{\mathrm{p},12}\cdot T_{12}} \tag{25}$$

Energy efficiency of nonhybrid cooling and drying system:

$$\eta_3=\frac{\dot{Q}_{\mathrm{eva}}+\dot{m}_{10}\cdot(h_{10}-h_{11})}{\dot{W}_{\mathrm{e},1}+\dot{W}_{\mathrm{e},3}+\dot{m}_9\cdot h_{1,\mathrm{a}}+\dot{Q}_{\mathrm{RHVT}}+\dot{m}_{12}\cdot c_{\mathrm{p},12}\cdot T_{12}} \tag{26}$$

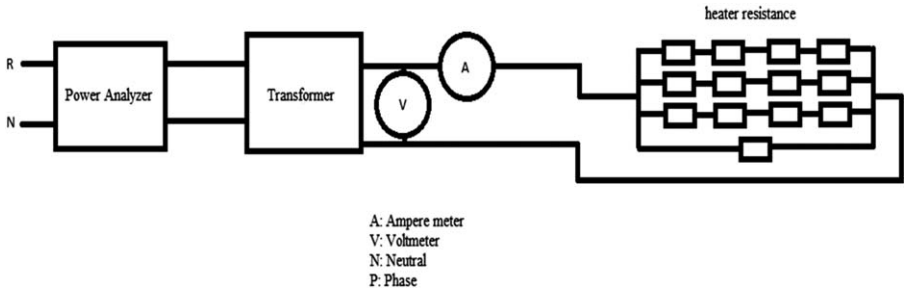

Figure 5. The electrical diagram of electrical heater [25].

a)

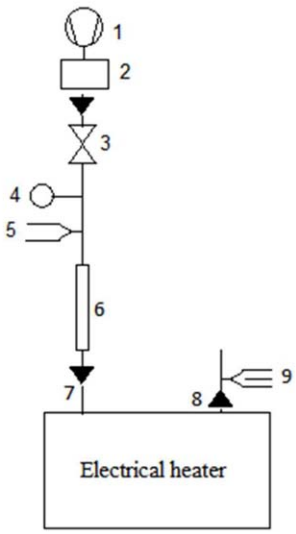

b)

Figure 6. The image (a) and schematic diagram (b) of the experimental set-up of the electrical heater [25]. [Color figure can be viewed at **wileyonlinelibrary.com**]

The exergy destruction for steady systems is given by the following equation:

$$\dot{E}x_{heat}+\dot{E}x_{in,m}-\dot{E}x_{out,m}-\dot{E}x_{work}=\dot{E}x_{d} \quad (27)$$

Here the exergy terms occurred by heat, mass, and work flow are given as follows:

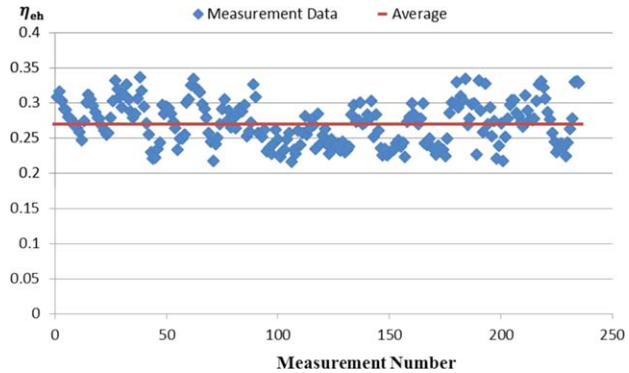

Figure 7. The experimental results of the electrical heater efficiency [25]. [Color figure can be viewed at **wileyonlinelibrary.com**]

Table 6. Mass composition ranges of tomato [28].

Constituents	% (*X*)
Water	93.76
Protein	0.85
Fat	0.33
Carbohydrate	3.54
Fiber	1.10
Ash	0.42

$$\dot{E}x_{heat}=\sum\left(1-\frac{T_0}{T_k}\right)\dot{Q}_k \quad (28)$$

$$\dot{E}x_{work}=\dot{W} \quad (29)$$

$$\dot{E}x_{in,m}=\sum\dot{m}_{in}\psi_{in} \quad (30)$$

$$\dot{E}x_{out,m}=\sum\dot{m}_{out}\psi_{out} \quad (31)$$

where ψ indicates the specific exergy term and given as

$$\psi=(h-h_0)-T_0(s-s_0) \quad (32)$$

where h is the enthalpy, s is the entropy, and the subscript zero indicates the properties of fluids at the dead state.

The exergy equations of the RHVTHCD system were obtained as follows:

Evaporator:

$$\dot{E}x_{d,eva}=\dot{m}_R\cdot(\Psi_5-\Psi_1)+\dot{Q}_{eva}\cdot\left(\frac{T_o}{T_1}-1\right) \quad (33)$$

Condenser:

$$\dot{E}x_{d,con}=\dot{m}_R\cdot(\Psi_2-\Psi_3)+\dot{Q}_{con}\cdot\left(1-\frac{T_o}{T_3}\right) \quad (34)$$

Heat exchanger:

$$\dot{E}x_{d,he}=\dot{m}_R\cdot(\Psi_3-\Psi_5)+\dot{m}_6\cdot(\Psi_6-\Psi_7)+\dot{Q}_{he}\cdot\left(1-\frac{T_0}{T_{he}}\right) \quad (35)$$

Cooling system compressor (C1):

$$\dot{E}x_{d,comp,1}=\dot{m}_R\cdot(\Psi_1-\Psi_2)+\dot{W}_{e,1} \quad (36)$$

RHVT compressor (C2):

$$\dot{E}x_{d,RHVT,comp,2}=\dot{m}_{1,a}\cdot\Psi_{1,a}-\dot{m}_8\cdot\Psi_8+\dot{W}_{e,2} \quad (37)$$

RHVT:

$$\dot{E}x_{d,RHVT}=\dot{m}_8\cdot\Psi_8-(\dot{m}_6\cdot\Psi_6+\dot{m}_7\cdot\Psi_7)+\dot{Q}_{RHVT}\cdot\left(\frac{T_o}{T_6}-1\right) \quad (38)$$

Throttling valve:

$$\dot{E}x_{d,tv}=\dot{m}_R\cdot(\Psi_3-\Psi_4) \quad (39)$$

Electrical heater:

$$\dot{E}x_{d,eh}=\dot{m}_9\cdot\Psi_9-\dot{m}_{10}\cdot\Psi_{10}+\dot{W}_{e,2} \quad (40)$$

Dryer:

$$\dot{E}x_{d,dry}=\dot{m}_{10}\cdot\Psi_{10}+\dot{m}_{12}\cdot\Psi_{12}-(\dot{m}_{11}\cdot\Psi_{11}+\dot{m}_{13}\cdot\Psi_{13}) \quad (41)$$

where Ψ indicates the specific exergy term and the specific exergy of the points in the RHVTHCD system are given in Eqs. (42–54).

$$\Psi_1=(h_1-h_0)-T_0\cdot(s_1-s_0) \quad (42)$$

$$\Psi_2=(h_2-h_0)-T_0\cdot(s_2-s_0) \quad (43)$$

$$\Psi_3=(h_3-h_0)-T_0\cdot(s_3-s_0) \quad (44)$$

$$\Psi_5=(h_{4a}-h_0)-T_0\cdot(s_5-s_0) \quad (45)$$

$$\Psi_6=c_{p6}\cdot\left[(T_6-T_0)-T_0\cdot\ln\frac{T_6}{T_0}\right]+R_a\cdot T_0\cdot\ln\left(\frac{P_6}{P_0}\right) \quad (46)$$

$$\Psi_7=(h_7-h_0)-T_0\cdot(s_7-s_0) \quad (47)$$

$$\Psi_{1,a}=\left[(c_p)_a+\omega_{1,a}\cdot(c_p)_v\right]\cdot(T_{1,a}-T_0)-T_0\cdot\left[\left[(c_p)_a+\omega_{1,a}\cdot(c_p)_v\right]\cdot\ln\left(\frac{T_{1,a}}{T_0}\right)-(R_a+\omega_{1,a}\cdot R_v)\cdot\ln\left(\frac{P_{1,a}}{P_0}\right)\right]+T_0\cdot\left[(R_a+\omega_{1,a}\cdot R_v)\cdot\ln\left(\frac{1+1.6078\cdot\omega_0}{1+1.6078\cdot\omega_{1,a}}\right)+1.6078\cdot\omega_{1,a}\cdot R_a\cdot\ln\left(\frac{\omega_{1,a}}{\omega_0}\right)\right] \quad (48)$$

$$\Psi_8=C_{p8}\cdot\left[(T_8-T_0)-T_0\cdot\ln\frac{T_8}{T_0}\right]+R_a\cdot T_0\cdot\ln\left(\frac{P_8}{P_0}\right) \quad (49)$$

$$\Psi_9=\left[(c_p)_a+\omega_9.(c_p)_v\right]\cdot(T_9-T_0)-T_0\cdot\left[\left[(c_p)_a+\omega_9\cdot(c_p)_v\right]\cdot\ln\left(\frac{T_9}{T_0}\right)-(R_a+\omega_9\cdot R_v)\cdot\ln\left(\frac{P_9}{P_0}\right)\right]+T_0\cdot\left[(R_a+\omega_9\cdot R_v)\cdot\ln\left(\frac{1+1.6078\cdot\omega_0}{1+1.6078\cdot\omega_9}\right)+1,6078\cdot\omega_9\cdot R_a\cdot\ln\left(\frac{\omega_9}{\omega_0}\right)\right] \quad (50)$$

$$\Psi_{10}=\left[(c_p)_a+\omega_{10}\cdot(c_p)_b\right]\cdot(T_{10}-T_0)-T_0\cdot\left[\left[(c_p)_a+\omega_{10}\cdot(c_p)_b\right]\cdot\ln\left(\frac{T_{10}}{T_0}\right)-(R_a+\omega_{10}\cdot R_v)\ln\left(\frac{P_{10}}{P_0}\right)\right]+T_0\cdot\left[(R_a+\omega_{10}\cdot R_v)\cdot\ln\left(\frac{1+1.6078\cdot\omega_0}{1+1.6078\cdot\omega_{10}}\right)+1.6078\cdot\omega_{10}\cdot R_a\cdot\ln\left(\frac{\omega_{10}}{\omega_0}\right)\right] \quad (51)$$

$$\Psi_{11}=\left[(c_p)_a+\omega_{11}\cdot(c_p)_v\right]\cdot(T_{11}-T_0)-T_0\cdot\left[\left[(c_p)_a+\omega_{11}\cdot(c_p)_v\right]\cdot\ln\left(\frac{T_{11}}{T_0}\right)-(R_a+\omega_{11}\cdot R_v)\cdot\ln\left(\frac{P_{11}}{P_0}\right)\right]+T_0\cdot\left[(R_a+\omega_{11}\cdot R_v)\ln\left(\frac{1+1.6078\cdot\omega_0}{1+1.6078\cdot\omega_{11}}\right)+1.6078\cdot\omega_{11}\cdot R_a\cdot\ln\left(\frac{\omega_{11}}{\omega_0}\right)\right] \quad (52)$$

$$\Psi_{12}=c_{p,12}\cdot\left[(T_{12}-T_0)-T_0\ln\frac{T_{12}}{T_0}\right] \quad (53)$$

$$\Psi_{13}=c_{p,13}\cdot\left[(T_{13}-T_0)-T_0\cdot\ln\frac{T_{13}}{T_0}\right] \quad (54)$$

where ω indicates the humidity ratio of air, reference dead state; $\omega^o=0.02023$ [29]. In the system $v\cong v_\infty$ and the changing of pressure is neglected [30] in drying system.

Exergetic efficiency of RHVTHCD system (ε_1):

$$\varepsilon_1=1-\frac{\dot{E}x_{d,eva}+\dot{E}x_{d,con}+\dot{E}x_{d,he}+\dot{E}x_{d,comp,1}+\dot{E}x_{d,RHVT,comp,2}+\dot{E}x_{d,RHVT}+\dot{E}x_{d,tv}+\dot{E}x_{d,eh}+\dot{E}x_{d,dry}}{\dot{m}_8\cdot\Psi_{1,a}+\dot{W}_{e,1}+\dot{W}_{e,2}+\dot{W}_{e,3}+\dot{Q}_{RHVT}\cdot\left(\frac{T_o}{T_6}-1\right)+\dot{Q}_{be}\cdot\left(1-\frac{T_0}{T_{he}}\right)+\dot{m}_{12}\cdot\Psi_{12}} \quad (55)$$

Exergetic efficiency of RHVTHCDW system (ε_2):

$$\varepsilon_2=1-\frac{\dot{E}x_{d,eva}+\dot{E}x_{d,con}+\dot{E}x_{d,he}+\dot{E}x_{d,comp,1}+\dot{E}x_{d,RHVT,comp,2}+\dot{E}x_{d,RHVT}+\dot{E}x_{d,tv}+\dot{E}x_{d,eh}+\dot{E}x_{d,dry}}{\dot{m}_8\cdot\Psi_8+\dot{W}_{e,1}+\dot{W}_{e,3}+\dot{Q}_{RHVT}\cdot\left(\frac{T_o}{T_6}-1\right)+\dot{Q}_{he}\cdot\left(1-\frac{T_0}{T_{he}}\right)+\dot{m}_{12}\cdot\Psi_{12}} \quad (56)$$

Table 7. The devices and unit costs [25,31].

Device	Cost (€)
Ranque–Hilsch vortex tube (C_{RHVT})	80
Heat exchanger (C_{he})	433.33
Cooling cabinet (C_{Cab})	1200
RHVT compressor ($C_{RHVT,comp}$)	1366.66
Dryer and electrical heater ($C_{dryer,eh}$)	8333.33

Exergetic efficiency of RHVTNHCD system (ε_3):

$$\varepsilon_3 = 1 - \frac{\dot{E}x_{d,eva} + \dot{E}x_{d,con} + \dot{E}x_{d,comp,1} + \dot{E}x_{d,tv} + \dot{E}x_{d,eh} + \dot{E}x_{d,dry}}{\dot{m}_9 \cdot \Psi_{1,a} + \dot{W}_{e,1} + \dot{W}_{e,3} + \dot{m}_{12} \cdot \Psi_{12}} \tag{57}$$

Economic Analysis

The life cycle cost ($C_{RHVTHCD}$) of RHVTHCD occurs by the investment costs (C_{ic}), salvage cost (C_{sc}), operating costs (C_{OC}), maintenance costs (C_{mc}), and benefit (C_b).

$$C_{RHVTHCD} = C_{sc} - C_{ic} + C_{mc} + C_b - C_{OC} \tag{58}$$

Investment costs (C_{ic});

$$C_{ic} = C_{RHVT} + C_{VCC} + C_{he} + C_{RHVT,comp} + C_{cab} + C_{dryer,eh} \tag{59}$$

where C_{RHVT} is the cost of Ranque–Hilsch vortex tube (€), C_{he} is the cost of heat exchanger (€),C_{Cab} is the cost of cooling cabinet (€),$C_{RHVT,comp}$ is the cost of RHVT compressor (€) and these devices costs are given in Table 7 and cost values are constant.

Cost of cooling system (C_{VCC}) is calculated with Eq. (60) [25,32]:

$$C_{VCC} = \left(253.99 \cdot \dot{Q}_{eva} + 2061.3\right) \tag{60}$$

The salvage cost of the hybrid system was taken as 10% of the investment cost [33,34].

$$C_{sc} = C_{ic} \cdot 0.10 \tag{61}$$

The maintenance cost of the hybrid system was taken as 2% of the investment cost of the hybrid system [33,34].

$$C_{mc} = C_{ic} \cdot 0.02 \tag{62}$$

The benefit of the hybrid system includes cooling and drying earnings.

$$C_b = \left(\frac{\dot{m}_{13,33} \cdot t_{33} + \dot{m}_{13,16} \cdot t_{16}}{t_{dp}}\right) \cdot 15.66 + \left(\frac{\left(\left(\dot{m}_{cp,33} \cdot t_{33}\right) + \left(\dot{m}_{cp,16} \cdot t_{16}\right)\right)}{3600 \cdot 24} \cdot 0.0047\right) \tag{63}$$

where $\dot{m}_{13,33}$ is the mass of dried product summer period (kg/s), t_{33} is the summer period (s), $\dot{m}_{13,16}$ is the mass of dried product winter period (kg/s), t_{16} is the winter period (s), $\dot{m}_{cp,33}$ is the cooled product summer period (kg/s), and $\dot{m}_{cp,16}$ is the cooled product winter period (kg/s). The unit price of dry product and cooled product is 15.66 €/kg and 0.0047 €/kg·h, respectively [35–38]. Operating costs of the system is given by

$$C_{OC} = C_e + C_{fp} \tag{64}$$

where C_e is the electrical costs of the hybrid system and C_{fp} is the fresh product costs which is dried in the drying system. Electrical costs are

$$C_e = \left(\left(\dot{W}_{e,1(33)} + \dot{W}_{e,2(33)} + \dot{W}_{e,3(33)}\right) \cdot t_{33}\right) + \left(\left(\dot{W}_{e,1(16)} + \dot{W}_{e,2(16)} + \dot{W}_{e,3(16)}\right) \cdot t_{16}\right) \cdot 0.107 \tag{65}$$

where 0.107 €/kW is the electrical energy [39].

The fresh product cost is

$$C_{fp} = \frac{\left(\left(\dot{m}_{12,33} \cdot t_{33}\right) + \left(\dot{m}_{12,16} \cdot t_{16}\right)\right)}{t_{dp}} \cdot 0.6 \tag{66}$$

where $\dot{m}_{12,33}$ is the mass of the fresh product summer period, $\dot{m}_{12,16}$ is the mass rate of the fresh product winter period, and 0.6 €/kg is the cost of 1 kg fresh product (tomatoes) [40].

The net cash flow is

$$C_T = \left(C_{fp} + C_b + C_e + C_{mc}\right) \cdot (1+i)^{t-1} \tag{67}$$

in this equation, i is the interest rate and t is the related year time of cash flow. The net present value (NPV) of hybrid system is given by

$$NPV = (C_{sc} + C_{ic}) + \sum_{t=0}^{ol} \frac{C_T}{(1+j)^t} \tag{68}$$

where ol is the operating life of the hybrid system and j is the discount rate. In this study, the operating life of the hybrid system has been added to calculations as 20 years. The discount and interest rates were taken as 9% and 7.25%, respectively [41,42].

RESULTS AND DISCUSSION

The experimental results of RHVT were used in the designing of the RHVTHCD system. The change of temperature differences between hot and cold outlet flows of RHVT ($\Delta T_{H\text{-}C}$) for the 0 type of RHVT are given Figure 8.

As seen in Figure 8, the control valve angle, RHVT body and inlet stream pressure of RHVT were kept constant the highest $\Delta T_{H\text{-}C}$ measured for the third control valve opening position. The control valve opening position, control valve angle and RHVT body kept constant the $_{\text{-}C}$ increased with increasing the inlet flow pressure of RHVT. $\Delta T_{H\text{-}C}$ values increase by the decrease of the control valve angle and by the increase of L/D value. The maximum $\Delta T_{H\text{-}C}$ was measured as 51 K for the third control valve opening position, 0 type RHVT generator, first RHVT body, P_8 of 601,325 kPa and control valve angle of 30°. For the same operating conditions temperature differences between inlet and cold outlet flow of RHVT (ΔT_C) was measured 22.3 K and the maximum temperature differences of hot flow and inlet flow of RHVT (ΔT_H) was measured same conditions as 27.7 K. The change of temperature differences between hot outlet flow and inlet flow of RHVT (ΔT_H) for control valve opening position and 0 type RHVT generator are given in Figure 9.

As seen in Figure 9, the control valve opening position, control valve angle, and RHVT body kept constant the ΔT_H increased with increasing the inlet flow pressure of RHVT. ΔT_H values increase by the decrease of the control valve angle and by the increase of L/D value. The maximum ΔT_H was measured as 27.7 K for the third control valve opening position, 0 type RHVT generator, first RHVT body, P_8 of 601,325 kPa and control valve angle of 30°. The change of temperature differences between cold outlet flow and inlet flow of RHVT (ΔT_C) for control valve opening position and N-type RHVT generator are given in Figure 10.

As seen in Figure 10, the control valve opening position, control valve angle and RHVT body kept constant the ΔT_C

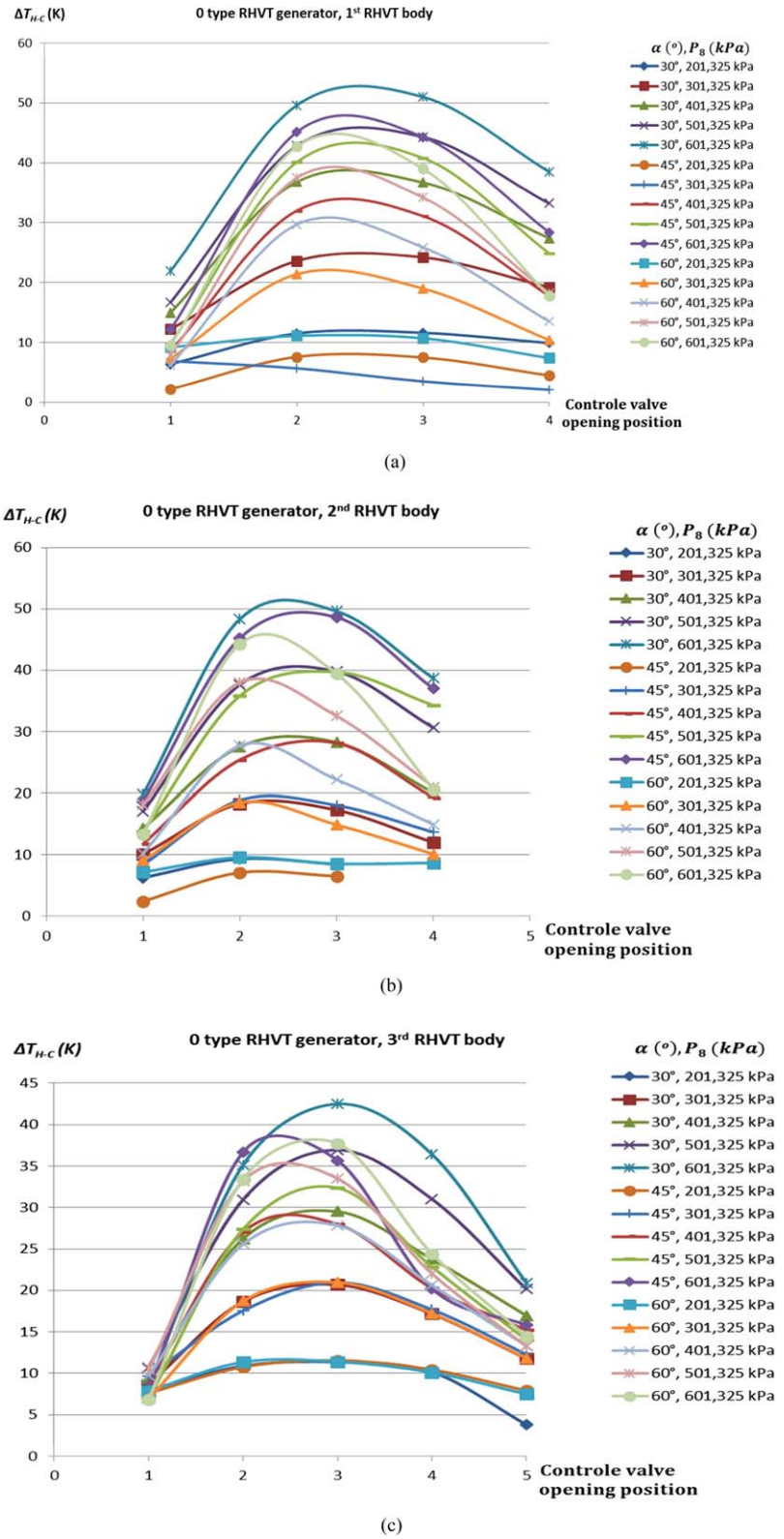

Figure 8. The change of $\Delta T_{H\text{-}C}$ for the control valve opening position of 0 type RHVT generator and (a) first RHVT body, (b) second RHVT body, and (c) third RHVT body. [Color figure can be viewed at **wileyonlinelibrary.com**]

increased with increasing the inlet flow pressure of RHVT. ΔT_C values increase by the increase of the control valve angle. The maximum ΔT_C was measured as 37.2 K for the second control valve opening position, N-type RHVT generator, second RHVT body, P_8 of 601,325 kPa and control valve angle of 30°. For the same operating conditions temperature differences between hot outlet flow and inlet flow of RHVT (ΔT_H) was measured 8.71 K and the maximum temperature differences of hot outlet flow and cold outlet flow of RHVT ($\Delta T_{H\text{-}C}$) was measured as 45.91 K.

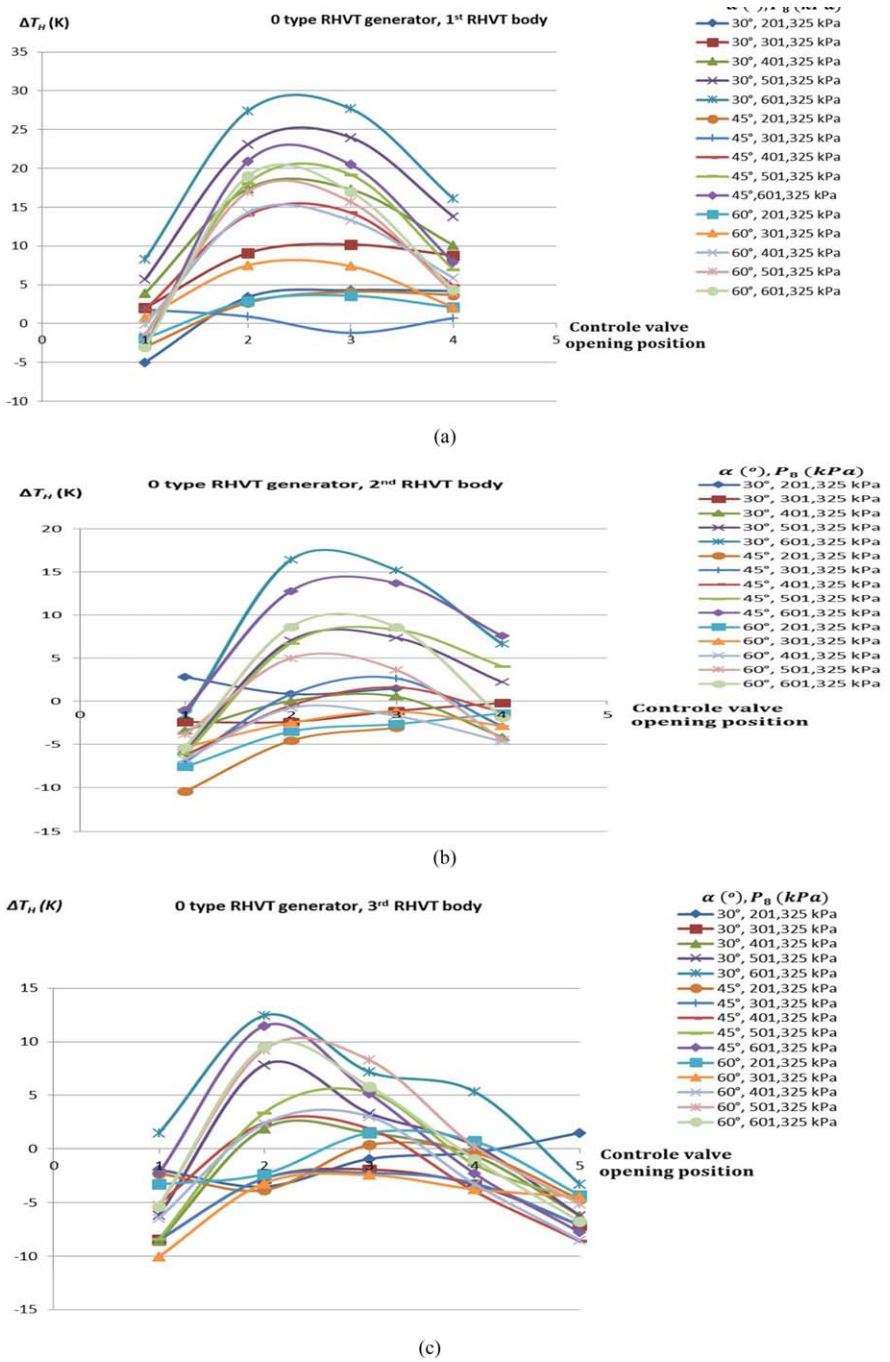

Figure 9. The change of ΔT_H for the control valve opening position of 0 type RHVT generator and (a) first RHVT body, (b) second RHVT body, and (c) third RHVT body. [Color figure can be viewed at **wileyonlinelibrary.com**]

Handling the operating parameters as R-134a, $T_{1,a}$ = 306.15 K, T_1 = 276,15 K, T_{10} = 328.15 K, T_{11} = 308.15 K, P_2 = 1300 kPa, RHVT generator type of J ($h/w = 0.25$, $d/D = 0.59$), $\alpha = 45°$, third control valve position, the variation of energy efficiency of the RHVTHCD ($\eta_{RHVTHCD}$) system with different inlet air pressure of RHVT (P_8) and RHVT body was obtained as seen in Figure 11.

According to Figure 11, the energy efficiency of RHVTHCD system of proposed RHVTHCD system ranges between 2.00% and 24.50%. The highest energy efficiency of RHVTHCD system value was obtained for first control valve opening position and 601.325kPa of the inlet flow pressure of RHVT. Handling the operating parameters as R-134a, $T_{1,a}$ = 306.15 K, T_1 = 276,15 K, T_{10} = 328.15 K, T_{11} = 308.15 K, P_2 = 1300 kPa, RHVT generator type of J ($h/w = 0.25$, $d/D = 0.59$), P_8 = 601.325, second RHVT body ($L/D = 29.17$), the variation of energy efficiency of the RHVTHCD ($\eta_{RHVTHCD}$) system with different control valve angle (α) and control valve opening position was obtained as seen in Figure 12.

As seen in Figure 12, the energy efficiency of RHVTHCD system highest value was obtained at the third control valve opening position when the control valve angle was kept constant. The highest energy efficiency value of RHVTHCD system was obtained as 4.65% for third control valve opening position and the control valve angle at 45°. The energy

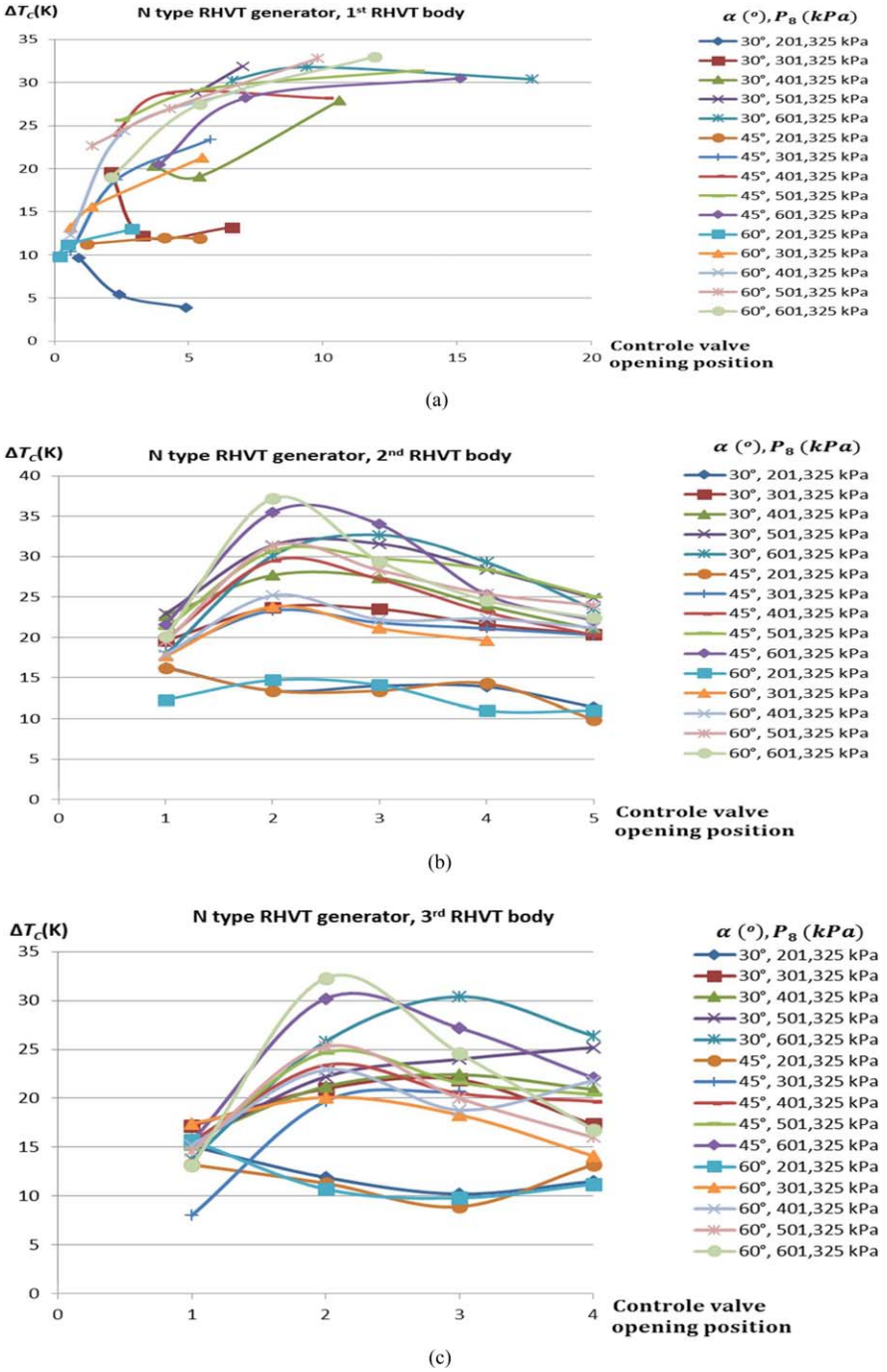

Figure 10. The change of ΔT_C for the control valve opening position of N-type RHVT generator and (a) first RHVT body, (b) second RHVT body, and (c) third RHVT body. [Color figure can be viewed at **wileyonlinelibrary.com**]

efficiency value of RHVTHCD system of proposed RHVTHCD system ranges between 4.20% and 4.65%. The change of the energy efficiency value of RHVTHCD system for R-134a, $T_{1,a}$ = 306.15 K, T_1 = 276.15 K, T_{10} = 328.15 K, T_{11} = 308.15 K, P_2 = 1300 kPa, RHVT generator type of J ($h/w = 0.25$, $d/D = 0.59$), P_8 = 501.325, first RHVT body ($L/D = 40$), third control valve position, $\alpha = 30°$ according to different type of RHVT generator are given in Figure 13.

As seen in Figure 13, the highest value of the energy efficiency of RHVTHCD system was obtained at N-type of RHVT generator ($h/w = 0.25$, $d/D = 0.43$) as 6.80%. The energy efficiency of RHVTHCD system increased with the decrease of h/w when the d/D ratio was kept constant. The changing of the energy efficiency value of RHVTHCD system for refrigerant as R-134a $T_{1,a}$ = 306.15 K, P_8 = 201.325 kPa, T_{10} = 328.15 K, T_{11} = 308.15 K, J type of RHVT generator ($h/w = 0.25$, $d/D = 0.59$), $\alpha = 30°$ and first RHVT body ($L/D = 40$), according to different compressor outlet pressure of refrigerant (P_2) and evaporator temperature (T_1) are given in Figure 14.

According to Figure 14, the energy efficiency of RHVTHCD system is being increased with increasing the evaporator temperature and decreasing the compressor outlet pressure of the refrigerant. The highest energy efficiency of RHVTHCD system value of proposed RHVTHCD system was obtained for 277.15 K of evaporator temperature and

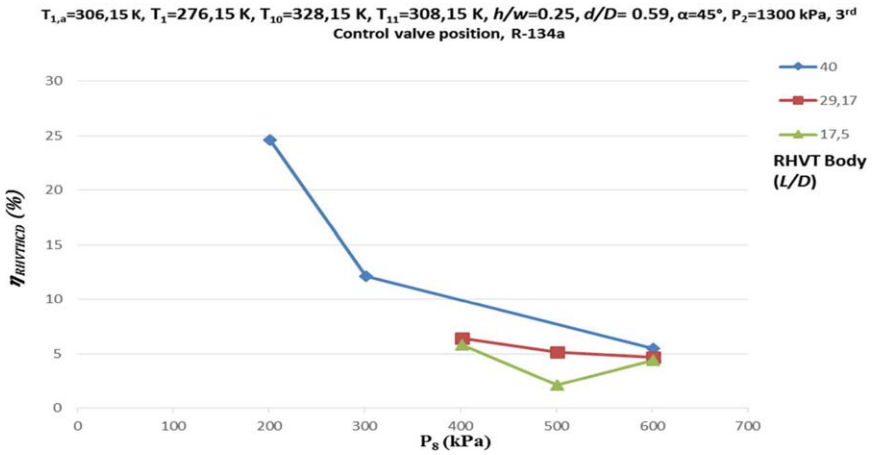

Figure 11. The variation of $\eta_{RHVTHCD}$ versus P_8 and RHVT body. [Color figure can be viewed at **wileyonlinelibrary.com**]

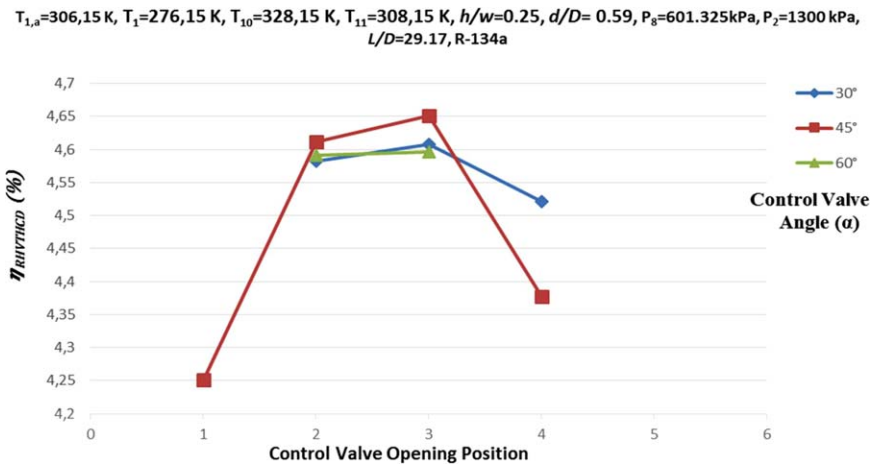

Figure 12. The variation of $\eta_{RHVTHCD}$ versus α and control valve opening position. [Color figure can be viewed at **wileyonlinelibrary.com**]

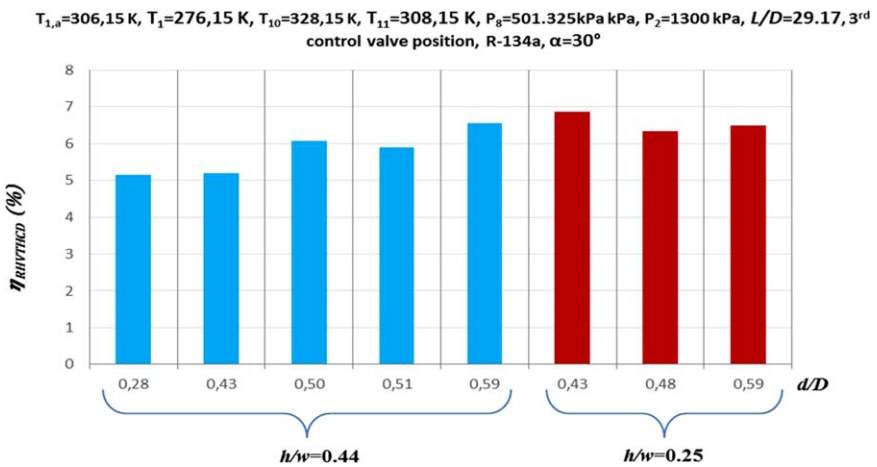

Figure 13. The variation of $\eta_{RHVTHCD}$ versus type of RHVT generator. [Color figure can be viewed at **wileyonlinelibrary.com**]

1300 kPa of the compressor outlet pressure of refrigerant as 24.70%. The changing of the energy efficiency value of RHVTHCD system for $T_{1,a}$ = 306.15 K, T_1 = 275.15 K, P_8 = 601.325 kPa, P_2 = 2000 kPa, 0 type of RHVT generator ($h/w = 0.44$, $d/D = 0.51$), $\alpha = 60°$, third control valve opening position and first RHVT body ($L/D = 40$), according to

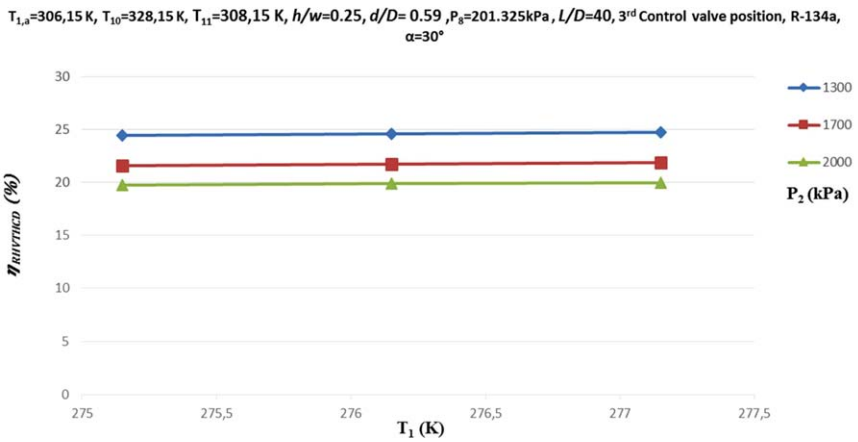

Figure 14. The variation of $\eta_{RHVTHCD}$ versus P_2 and T_1. [Color figure can be viewed at **wileyonlinelibrary.com**]

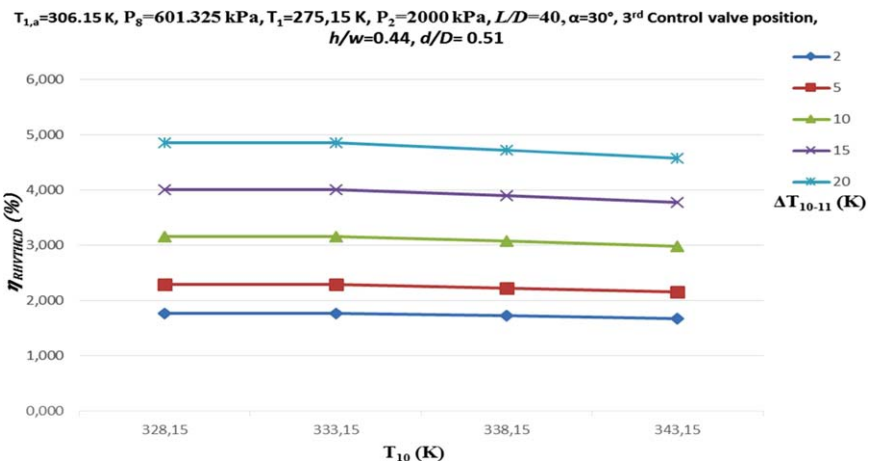

Figure 15. The variation of $\eta_{RHVTHCD}$ versus T_{10} and ΔT_{10-11}. [Color figure can be viewed at **wileyonlinelibrary.com**]

different inlet stream temperature of dryer and temperature differences between of inlet and outlet streams of dryer (ΔT_{10-11}) are given in Figure 15.

According to Figure 15, the energy efficiency of RHVTHCD system is being increased with increasing the temperature differences between of inlet and outlet streams of the dryer when the inlet stream temperature of the dryer was kept constant. The energy efficiency of RHVTHCD system is being increased with decreasing the inlet stream temperature of the dryer up to 328.15 K. The energy efficiency values of proposed RHVTHCD system range between 1.66 and 4.85%. The changing of the energy efficiency value of the system for $T_{1,a}$ = 306.15 K, T_1 = 276.15 K, P_8 = 501.325 kPa, T_{10} = 328.15 K, T_{11} = 308.15 K, 0 type of RHVT generator ($h/w = 0.44$, $d/D = 0.51$), $\alpha = 45°$, third control valve opening position and first RHVT body ($L/D = 40$) according to different refrigerant and system configuration are given in Figure 16.

According to Figure 16, the energy efficiency value of proposed system range between 4.97% and 7.14%. The highest energy efficiency value was obtained as 7.14% for NCDS and R-143a. For the same system parameters, the energy efficiency of the RHVTHCD and RHVTHCDW systems were calculated as 5.22% and 5.81%, respectively. The minimum exergy efficiency of the system was calculated as 4.97% for the RHVTHCD system and refrigerant of R-507a. For the same conditions the energy efficiency of the RHVTHCDW system and NCDS were obtained as 5.54% and 6.80%, respectively. Handling the operating parameters as R-134a, $T_{1,a}$ = 306.15 K, T_1 = 276,15 K, T_{10} = 328.15 K, T_{11} = 308.15 K, P_2 = 1300 kPa, RHVT generator type of J ($h/w = 0.25$, $d/D = 0.59$), $\alpha = 45°$, third control valve position, the variation of exergy efficiency of the RHVTHCD ($\varepsilon_{RHVTHCD}$) system with different inlet air pressure of RHVT (P_8) and RHVT body was obtained as seen in Figure 17.

According to Figure 17, the exergy efficiency of RHVTHCD system of proposed RHVTHCD system ranges between 0.30% and 5.99%. The highest exergy efficiency of RHVTHCD system value was obtained for first control valve opening position and 201.325kPa of the inlet flow pressure of RHVT. Handling the operating parameters as R-134a, $T_{1,a}$ = 306.15 K, T_1 = 276,15 K, T_{10} = 328.15 K, T_{11} = 308.15 K, P_2 = 1300 kPa, RHVT generator type of J ($h/w = 0.25$, $d/D = 0.59$), P_8 = 601.325, second RHVT body ($L/D = 29.17$), the variation of exergy efficiency of the RHVTHCD ($\varepsilon_{RHVTHCD}$) system with different control valve angle (α) and control valve opening position was obtained as seen in Figure 12.

As seen in Figure 18, the exergy efficiency of RHVTHCD system highest value was obtained at the second control valve opening position when the control valve angle was kept constant. The highest exergy efficiency value of RHVTHCD system was obtained as 0.434% for second control valve opening position and the control valve angle at

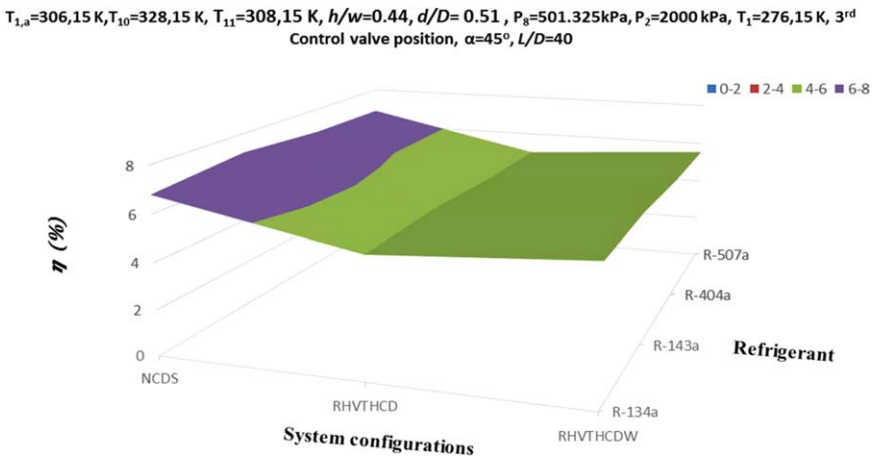

Figure 16. The variation of the energy efficiency of the system versus the system configuration and refrigerant. [Color figure can be viewed at **wileyonlinelibrary.com**]

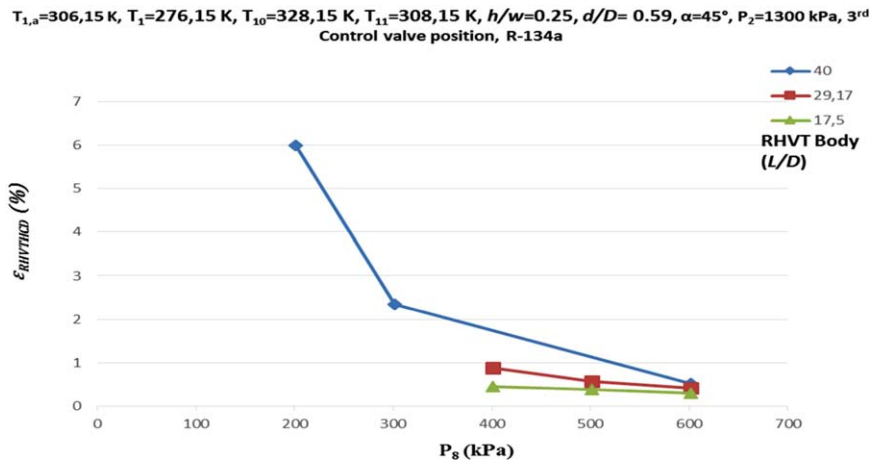

Figure 17. The variation of $\varepsilon_{RHVTHCD}$ versus P_8 and RHVT body. [Color figure can be viewed at **wileyonlinelibrary.com**]

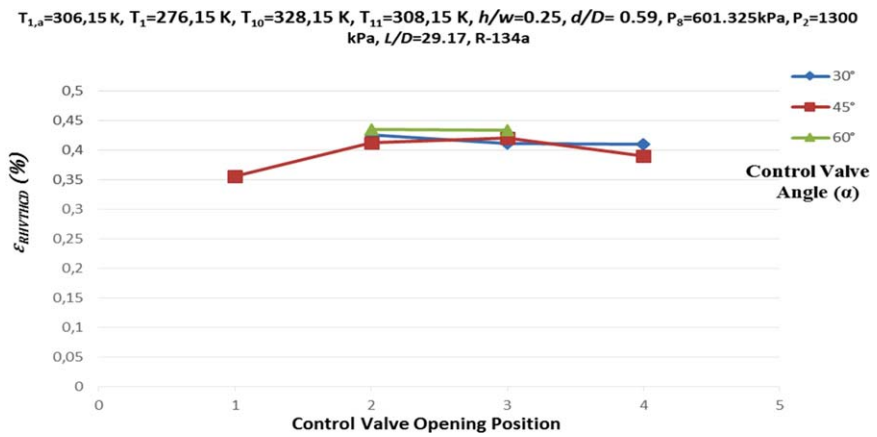

Figure 18. The variation of $\varepsilon_{RHVTHCD}$ versus α and control valve opening position. [Color figure can be viewed at **wileyonlinelibrary.com**]

60°. The exergy efficiency value of RHVTHCD system of proposed RHVTHCD system ranges between 0.35% and 0.43%. The change of the exergy efficiency value of RHVTHCD system for R-134a, $T_{1,a}$ = 306.15 K, T_1 = 276.15 K, T_{10} = 328.15 K, T_{11} = 308.15 K, P_2 = 1300 kPa, RHVT generator type of J ($h/w = 0.25$, $d/D = 0.59$), P_8 = 501.325, first

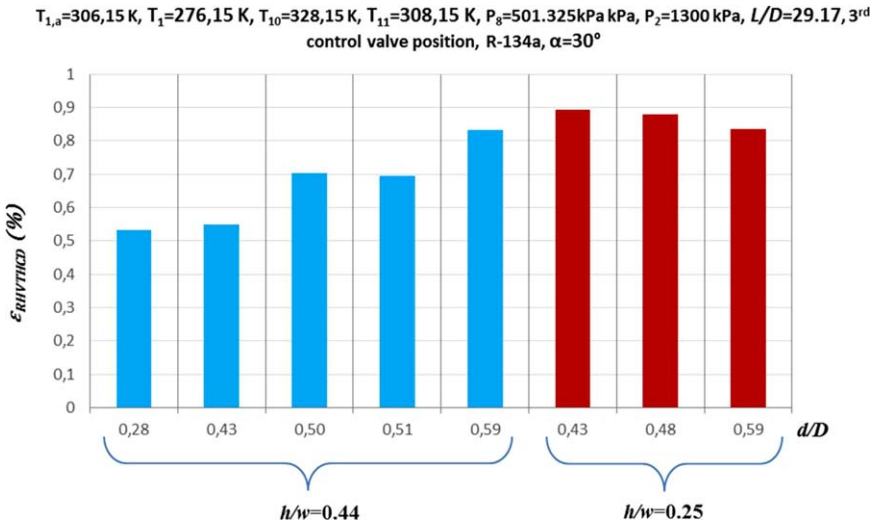

Figure 19. The variation of $\varepsilon_{RHVTHCD}$ versus type of RHVT generator. [Color figure can be viewed at **wileyonlinelibrary.com**]

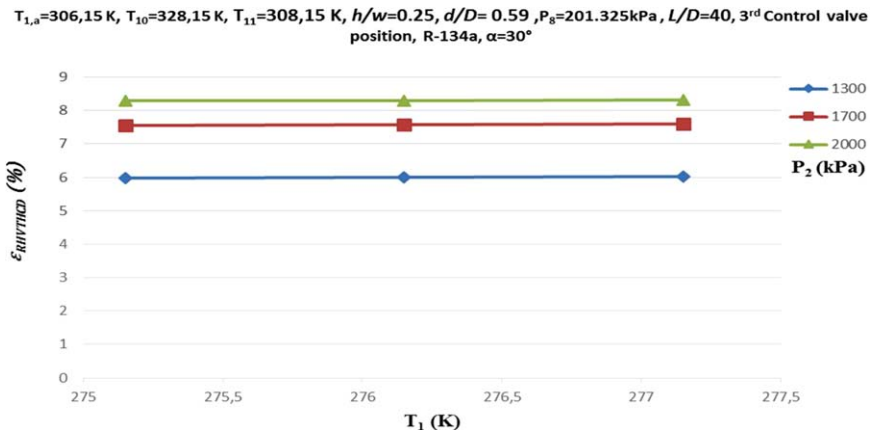

Figure 20. The variation of $\varepsilon_{RHVTHCD}$ versus P_2 and T_1. [Color figure can be viewed at **wileyonlinelibrary.com**]

RHVT body ($L/D = 40$), third control valve position, $\alpha = 30°$ according to different type of RHVT generator are given in Figure 19.

As seen in Figure 19, the highest value of the exergy efficiency of RHVTHCD system was obtained at N-type of RHVT generator ($h/w = 0.25$, $d/D = 0.43$) as 0.894%. The exergy efficiency of RHVTHCD system increased with the decrease of h/w when the d/D ratio was kept constant. The changing of the exergy efficiency value of RHVTHCD system for refrigerant as R-134a $T_{1,a}$ = 306.15 K, P_8 = 201.325 kPa, T_{10} = 328.15 K, T_{11} = 308.15 K, J type of RHVT generator ($h/w = 0.25$, $d/D = 0.59$), $\alpha = 30°$ and first RHVT body ($L/D = 40$) according to different compressor outlet pressure of refrigerant (P_2) and evaporator temperature (T_1) are given in Figure 20.

According to Figure 20, the exergy efficiency of RHVTHCD system is being increased with increasing the evaporator temperature and the compressor outlet pressure of the refrigerant. The highest exergy efficiency of RHVTHCD system value of proposed RHVTHCD system was obtained for 277.15 K of evaporator temperature and 2000 kPa of the compressor outlet pressure of refrigerant as 8.32%. The changing of the exergy efficiency value of RHVTHCD system for $T_{1,a}$ = 306.15 K, T_1 = 275.15 K, P_8 = 601.325 kPa, P_2 = 2000 kPa, 0 type of RHVT generator ($h/w = 0.44$, $d/D = 0.51$), $\alpha = 60°$, third control valve opening position and first RHVT body ($L/D = 40$) according to different inlet stream temperature of dryer and temperature differences between of inlet and outlet streams of dryer (ΔT_{10-11}) are given in Figure 21.

According to Figure 21, the exergy efficiency of RHVTHCD system is being increased with decreasing the temperature differences between of inlet and outlet streams of the dryer and increasing the inlet stream temperature of the dryer. The exergy efficiency values of proposed RHVTHCD system range between 0.60% and 1.77%. The changing of the exergy efficiency value of the system for $T_{1,a} = 306.15$ K, $T_1 = 276.15$ K, $P_8 = 501.325$ kPa, $T_{10} = 328.15$ K, $T_{11} = 308.15$ K, 0 type of RHVT generator ($h/w = 0.44$, $d/D = 0.51$), $\alpha = 45°$, third control valve opening position and first RHVT body ($L/D = 40$) according to different refrigerant and system configuration are given in Figure 22.

According to Figure 22, the exergy efficiency value of proposed system range between 0.38% and 1.85%. The highest exergy efficiency value was obtained as 1.85% for the R-134a and NCDS. For the same system parameters, the exergy efficiency of the RHVTHCD and RHVTHCDW systems were

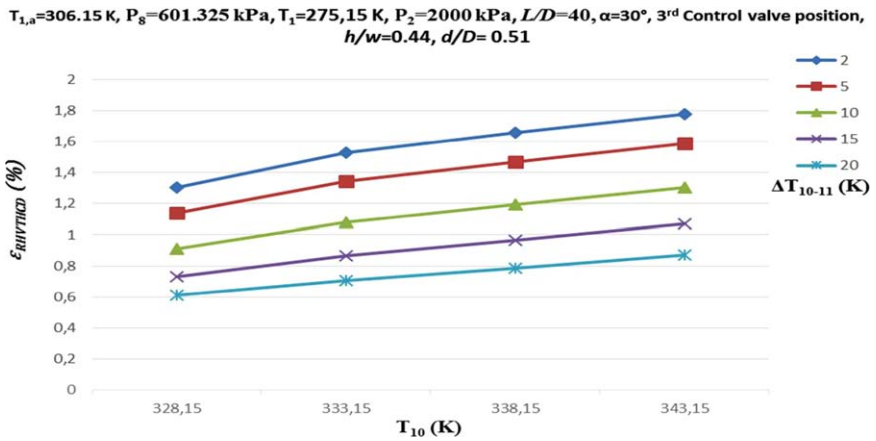

Figure 21. The variation of $\varepsilon_{RHVTHCD}$ versus T_{10} and ΔT_{10-11}. [Color figure can be viewed at **wileyonlinelibrary.com**]

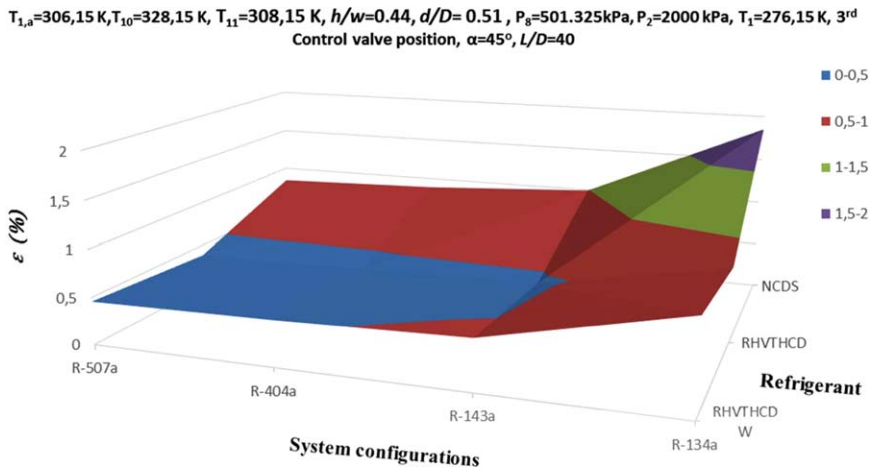

Figure 22. The variation of the exergy efficiency of the system versus the system configuration and refrigerant. [Color figure can be viewed at **wileyonlinelibrary.com**]

calculated as 0.79% and 0.96%, respectively. The minimum exergy efficiency of the RHVTHCD system was calculated as 0.38% for the RHVTHCD system and refrigerant of R-507a. For the same conditions the exergy efficiency of the RHVTHCDW system and NCDS were obtained as 0.45% and 0.84%, respectively. Handling the operating parameters as R-134a, $T_{1,a}$ = 306.15 K, T_1 = 276,15 K, T_{10} = 328.15 K, T_{11} = 308.15 K, P_2 = 1300 kPa, RHVT generator type of J ($h/w = 0.25$, $d/D = 0.59$), $\alpha = 45°$, third control valve position, the variation of NPV of the RHVTHCD system with different inlet air pressure of RHVT (P_8) and RHVT body was obtained as seen in Figure 23.

According to Figure 23, the NPV of RHVTHCD system of proposed RHVTHCD system ranges between −17441€and 6503 €. The highest exergy efficiency of RHVTHCD system value was obtained for second control valve opening position and 401.325kPa of the inlet flow pressure of RHVT as 6503 €. Handling the operating parameters as R-134a, $T_{1,a}$ = 306.15 K, T_1 = 276,15 K, T_{10} = 328.15 K, T_{11} = 308.15 K, P_2 = 1300 kPa, RHVT generator type of J ($h/w = 0.25$, $d/D = 0.59$), P_8 = 601.325, second RHVT body ($L/D = 29.17$) according to different control valve angle (α) and control valve opening position was obtained as seen in Figure 24.

As seen in Figure 24, the NPV of RHVTHCD system highest value was obtained at the second control valve opening position when the control valve angle was kept constant. The highest NPV value of RHVTHCD system of proposed RHVTHCD system was obtained as −788.67 for second control valve opening position and the control valve angle at 30°. The NPV value of RHVTHCD system of proposed RHVTHCD system ranges between −41967 €and −788.67€. The change of the NPV value of RHVTHCD system for R-134a, $T_{1,a}$ = 306.15 K, T_1 = 276.15 K, T_{10} = 328.15 K, T_{11} = 308.15 K, P_2 = 1300 kPa, RHVT generator type of J ($h/w = 0.25$, $d/D = 0.59$), P_8=501.325, first RHVT body ($L/D = 40$), third control valve position, $\alpha = 30°$ according to different type of RHVT generator are given in Figure 25.

As seen in Figure 25, the highest value of the NPV of RHVTHCD system was obtained at 0 type of RHVT generator ($h/w = 0.44$, $d/D = 0.51$) as 27354.86 €. The changing of the NPV value of RHVTHCD system for refrigerant as R-134a $T_{1,a}$ = 306.15 K, P_8 = 201.325 kPa, T_{10} = 328.15 K, T_{11} = 308.15 K, J type of RHVT generator ($h/w = 0.25$, $d/D = 0.59$), $\alpha = 30°$ and first RHVT body ($L/D = 40$) according to different compressor outlet pressure of refrigerant (P_2) and evaporator temperature (T_1) are given in Figure 26.

According to Figure 26, the NPV of RHVTHCD system is being increased with decreasing the evaporator temperature and decreasing the compressor outlet pressure of the refrigerant. The highest NPV of RHVTHCD system value of proposed RHVTHCD system was obtained for 275.15 K of

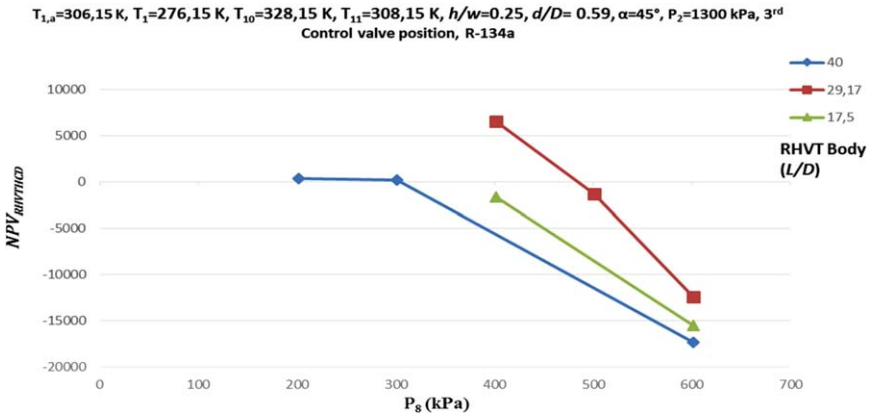

Figure 23. The variation of *NPV* versus P_8 and RHVT body. [Color figure can be viewed at **wileyonlinelibrary.com**]

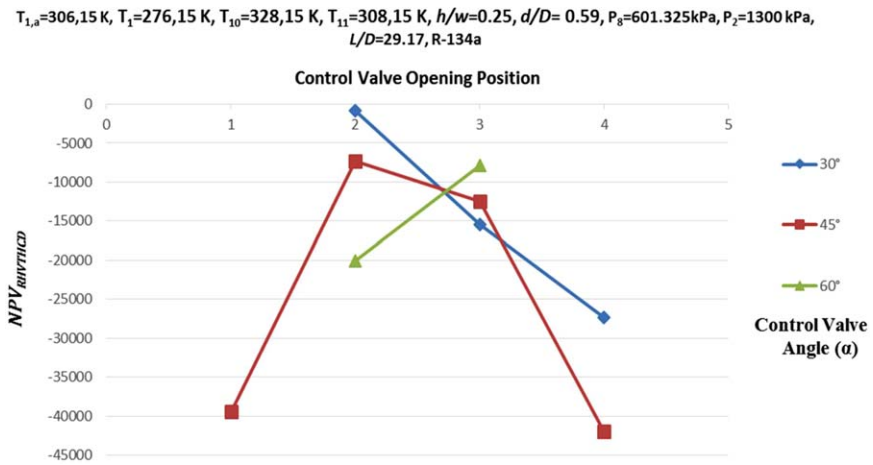

Figure 24. The variation of NPV versus α and control valve opening position. [Color figure can be viewed at **wileyonlinelibrary.com**]

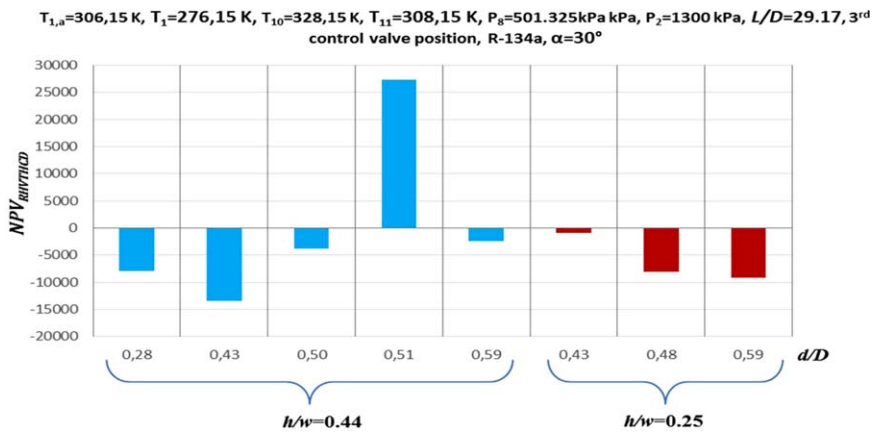

Figure 25. The variation of NPV versus type of RHVT generator. [Color figure can be viewed at **wileyonlinelibrary.com**]

evaporator temperature and 2000 kPa of the compressor outlet pressure of refrigerant as 301.90 €. The changing of the NPV value of RHVTHCD system for $T_{1,a}$ = 306.15 K, T_1 = 275.15 K, P_8 = 601.325 kPa, P_2 = 2000 kPa, 0 type of RHVT generator ($h/w = 0.44$, $d/D = 0.51$), $\alpha = 60°$, third control valve opening position and first RHVT body ($L/D = 40$)

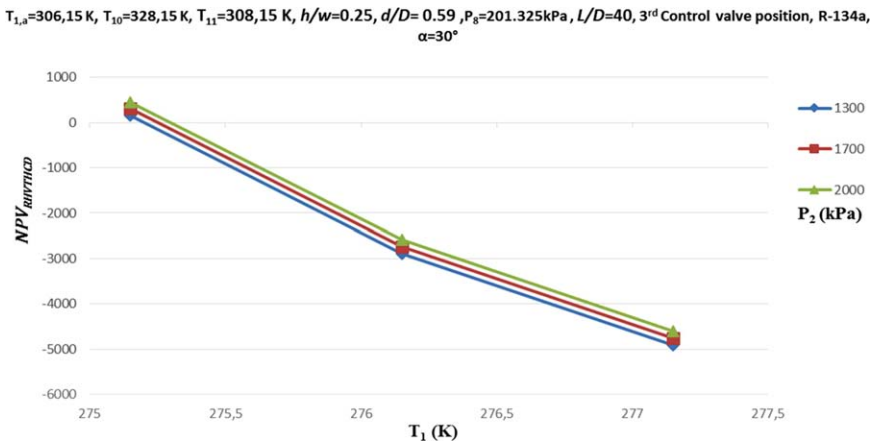

Figure 26. The variation of NPV versus P_2 and T_1. [Color figure can be viewed at **wileyonlinelibrary.com**]

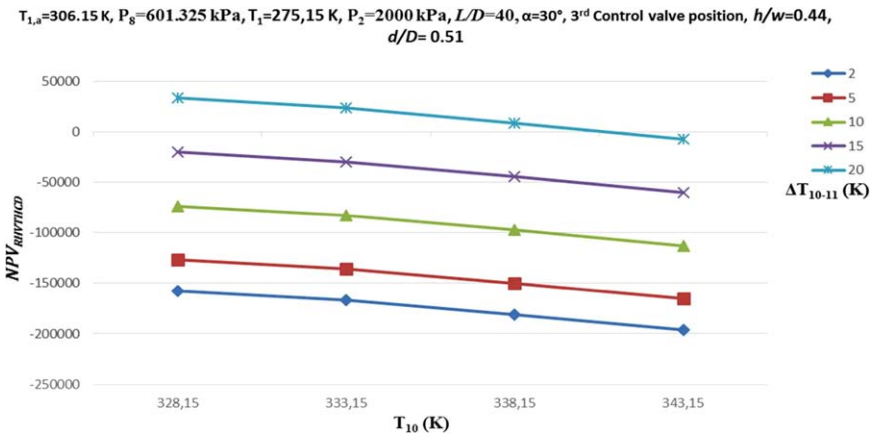

Figure 27. The variation of NPV versus T_{10} and ΔT_{10-11}. [Color figure can be viewed at **wileyonlinelibrary.com**]

according to different inlet stream temperature of dryer and temperature differences between of inlet and outlet streams of dryer (ΔT_{10-11}) are given in Figure 27.

According to Figure 27, the NPV of RHVTHCD system is being increased with increasing the temperature differences between of inlet and outlet streams of the dryer and decreasing the inlet stream temperature of the dryer. The NPV values of proposed RHVTHCD system range between −196196 € and 33962.05 €. The changing of the NPV value of the system for $T_{1,a} = 306.15$ K, $T_1 = 276.15$ K, $P_8 = 501.325$ kPa, $T_{10} = 328.15$ K, $T_{11} = 308.15$ K, 0 type of RHVT generator ($h/w = 0.44$, $d/D = 0.51$), $\alpha = 45°$, third control valve opening position and first RHVT body ($L/D = 40$) according to different refrigerant and system configuration are given in Figure 28.

According to Figure 28, the NPV value of proposed system range between 74.49 €and 103878.60 €. The highest NPV value was obtained for while using the R-143a and RHVTHCDW system as 311635.80 €. For the same system parameters, the NPV value of the RHVTHCD and RHVTHCDW systems were calculated as 3009.12 €and 103878.60 €, respectively. The minimum NPV value of the system was calculated as 74.49 for the RHVTHCD system and refrigerant of R-507a. For the same conditions the exergy efficiency of the RHVTHCDW system and NCDS were obtained as 100944 €and 97145.86 €, respectively.

According to the energy analysis results, the most effective RHVT body, refrigerant, helical vortex generator, control valve angle and control valve opening position are first ($L/D = 40$), R-134a, J type ($h/w = 0.25$, $d/D = 0.59$), 45° and third respectively for the RHVTHCD system. The maximum energy efficiency of RHVTHCD system was determined as 0.2474 for the ambient temperature of 306.15 K. These system properties were T_1 of 277.15 K, P_2 of 1300 kPa, T_{10} of 328.15 K, T_{11} of 308.15 K, and P_8 of 201.325 kPa. Under the same conditions, the exergy efficiency of the RHVTHCD system was calculated as 6.01% and 4.61% for the summer mode and winter mode, respectively. The NPV of this system was calculated as 453.61 €. For the same operating conditions, the energy efficiency of the NCDS was calculated as 32.12% and 5.89% at the ambient temperature of 306.15 K and 289.15 K, respectively. The energy efficiency of RHVTHCDW system is determined as 22.82% and 20.89% for the summer mode and winter mode, respectively.

According to the economic analysis results, the most effective RHVT body, refrigerant, helical vortex generator, control valve angle and control valve opening position are first ($L/D = 40$), R-134a, 0 type ($h/w = 0.44$, $d/D = 0.51$), 30° and third respectively for the RHVTHCD system. The maximum NBD of RHVTCD system was determined as 37256.63 €. These system properties were T_1 of 277.15 K, P_2 of 1300 kPa, T_{10} of 328.15 K, T_{11} of 308.15 K and P_8 of 601.325 kPa.

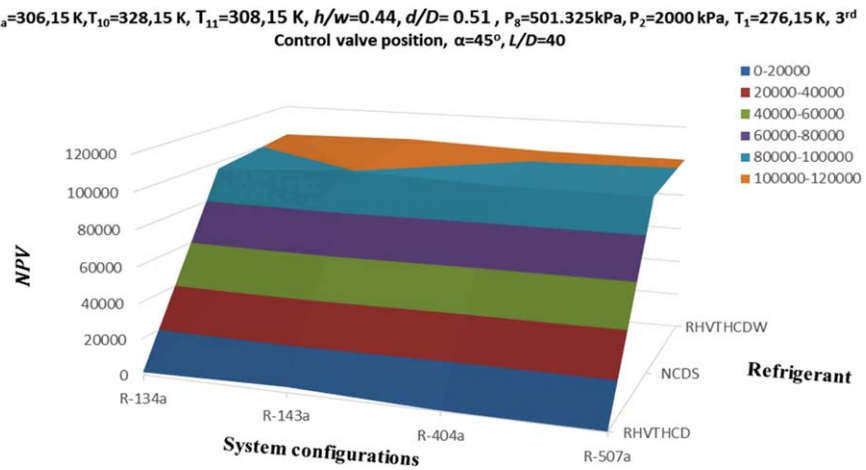

Figure 28. The variation of NPV of the system versus the system configuration and refrigerant. [Color figure can be viewed at **wileyonlinelibrary.com**]

Under the same conditions, the energy efficiency of the RHVTHCD system was calculated as 5.00% and 4.94% for the summer mode and winter mode, respectively. Exergy efficiency of this system was 0.42% and 0.44% for the summer mode and winter mode, respectively. For the same operating conditions, the energy efficiency of the NCDS was calculated as 6.65% and 4.58% at the ambient temperature of 306.15 K and 289.15 K, respectively. The energy efficiency of RHVTHCDW system is determined as 5.80 and 5.59 for the summer mode and winter mode, respectively. Under the same operating conditions, the NPV of the NCDS and RHVTHCDW system were calculated as 188442.50 €and 199863.40 €. For the same operating conditions and RHVT geometries, the highest NPV was obtained for the RHVTHCDW system which is used waste air for inlet stream of RHVT.

CONCLUSION

The NPV of the RHVTHCD system increased with the decrease of the inlet stream pressure of RHVT, the compressor outlet pressure of the refrigerant, the temperature differences between the inlet and outlet dryer air, and the decrease of the inlet temperature of the dryer and evaporator temperature. The highest NPV value of the RHVTHCD system was obtained for 30° control valve angle and third control valve opening position. The energy and exergy efficiencies of RHVTHCD system increase with the increase of the evaporator temperature. The increase of the temperature differences between inlet and outlet dryer air causes to increase energy efficiency and the decrease of exergy efficiency of the RHVTHCD system.

ACKNOWLEDGMENT

This study was supported by Scientific Research Projects Unit of Dumlupinar University (DPUBAP) with the project no of 2013/5.

NOMENCLATURE

C	Cost (€)
COP	Coefficient of performance
c	Specific heat (kJ/kg K)
D	Diameter of RHVT body (mm)
d	Inner diameter of the generator (mm)
$\dot{E}x$	Exergy (kW)
h	Specific enthalpy (kJ/kg)
i	Interest rate (%)
j	Discount rate (%)
L	Length of the RHVT body (mm)
$\dot{m}$	Mass flow (kg/s)
MR	Moisture ratio
n	The numbers of measurement
NPV	Net present value (€)
P	Pressure (kPa)
ol	Operating life (year)
R	Gas constant (kPa · m^3/kg · K)
$\dot{Q}$	Heat energy (kJ/s)
s	Specific entropy (kJ/kg · K)
SD	Standard deviation
t_{16}	Working time of the system for winter (h)
t_{16}	Working time of the system for summer (h)
t	Time (year)
T	Temperature (K)
U	Uncertainty
ω	Humidity ratio
w	Width of the generator channel (mm)
$\dot{W}$	Electrical power (kJ/s)
$\bar{X}$	The average of the measurement
X_m	The measurement
η	Energy efficiency (%)
ε	Exergy efficiency (%)
ψ	Specific exergy (kJ/kg)
α	Control valve angle (°)

Subscripts

a	Air
ash	Ash
b	Benefit
Cab	Cooling cabinet
car	Carbohydrate
comp	Compressor
con	Condenser
cp	Cooled product
d	Destruction
dp	Dried product
dry	Dryer
e	Electrical
eh	Electrical heater
eva	Evaporator
exp	Experimental
fat	Fat
fib	Fiber
fp	Fresh product
he	Heat exchanger
ic	Investment costs
in	Inlet

m	Mass
mc	Maintenance costs
mec	Mechanical
NCDS	Nonhybrid cooling and drying system
oc	Operating costs
out	Outlet
pro	Protein
R	Refrigerant
RHVT	Ranque–Hilsch vortex tube
RHVTHCD	Ranque–Hilsch vortex tube aided hybrid cooling and drying system
RHVTHCDW	Ranque–Hilsch vortex tube aided hybrid cooling and drying system in which used the input stream of RHVT is obtained from the different system as a waste
sc	Salvage costs
T	Total
t	Time (year)
tom	Tomato
tv	Throttling valve
v	Vapor
VCC	Vapor compression cooling
w	Water
0	Dead state
16	Winter period
33	Summer period

LITERATURE CITED

1. Esper, A., & Muhlbauer, W. (1998). *Solar drying- an effective means of food preservation*, Renewable Energy, 15, 95–100.
2. Khoshnevisan, B., Bolandnazar, E., Shamshirband, S., Motamed Shariati, H., Anuar, N.B., & Kiah, M.L.M. (2015). *Decreasing environmental impacts of cropping systems using life cycle assessment (LCA) and multi-objective genetic algorithm*, Journal of Cleaner Production, 86, 67–77.
3. Sajjadi, S., Shamshirband, S., Alizamir, M., Yee, P.L., Mansor, Z., Manaf, A.A., Altameem, T.A., & Mostafaeipour, A. (2016). *Extreme learning machine for prediction of heat load in district heating systems*, Energy and Buildings, 122, 222–227.
4. Aghbashlo, M., Shamshirband, S., Tabatabaei, M., Yee, P.L., & Larimi, Y.N. (2016). *The use of ELM-WT (extreme learning machine with wavelet transform algorithm) to predict exergetic performance of a DI diesel engine running on diesel/biodiesel blends containing polymer waste*, Energy, 94, 443–456.
5. Ranque, G.J. (1933). *Experiences sur la detente giratoire avec production simulanees 'un echappement d'air chaud et d'air froid*, Journal de Physique et Le Radium (in French), 7, 112–114.
6. Saidi, M.H., & Valipour, M.S. (2003). *Experimental modeling of vortex tube refrigerator*, Applied Thermal Engineering, 23, 1971–1980.
7. Pourmahmoud, N., Hassanzadeh, A., & Moutaby, O. (2012). *Numerical analysis of the effect of helical nozzles gap on the cooling capacity of Ranque–Hilsch vortex tube*, International Journal of Refrigeration, 35, 1473–1483.
8. Xue, Y., Arjomandi, M., & Kelso, R. (2014). *Energy analysis within a vortex tube*, Experimental Thermal and Fluid Science, 52, 139–145.
9. Kırmacı, V. (2009). *Exergy analysis and performance of a counter flow Ranque–Hilsch vortex tube having various nozzle numbers at different inlet pressures of oxygen and air*, International Journal of Refrigeration, 32, 1626–1633.
10. Sommers, A.D., & Jacobi, A.M. (2005). *Air-side heat transfer enhancement of a refrigerator evaporator using vortex generation*, International Journal of Refrigeration, 28, 1006–1017.
11. AYDIN, O., & BAKI, M. (2006). *An experimental study on the design parameters of a counterflow vortex tube*, Energy, 31, 2763–2772.
12. Dincer, K., & Baskaya, S. (2009). *Assessment of plug angle effect on exergy efficiency of counterflow Ranque–Hilsch vortex tubes with the exergy analysis method*, Journal of the Faculty of Engineering and Architecture of Gazi University, 24, 533–538. Vol No
13. Kabeel, A.E., Sultan, G.I., Zyada, Z.A., & El-Hadary, M.I. (2010). *Performance study of spot cooling of tractor cabinet*, Energy, 35, 1679–1687.
14. Rafiee, S.E., & Sadeghiazad, M.M. (2017). *Experimental and 3D CFD investigation on heat transfer and energy separation inside a counter flow vortex tube using different shapes of hot control valves*, Applied Thermal Engineering, 110, 648–664.
15. A., Kumar, Vivekanand, S. & Subudhi, (2017). *Cooling and dehumidification using vortex tube*, Applied Thermal Engineering, 122, 181–193.
16. Cebeci, I., Kırmacı, V., & Topcuoglu, U. (2016). *The effects of orifice nozzle number and nozzle made of polyamide plastic and aluminum with different inlet pressures on heating and cooling performance of counter flow Ranque–Hilsch vortex tubes: An experimental investigation*, International Journal of Refrigeration, In Press, Accepted Manuscript, **https://doi.org/doi**:10.1016/j.ijrefrig.2016.07.013.
17. Dutta, T., Sinhamahapatra, K.P., & Bandyopadhyay, S.S. (2011). *Numerical investigation of gas species and energy separation in the Ranque–Hilsch vortex tube using real gas model*, International Journal of Refrigeration, 34, 2118–2128.
18. Thakare, H.R., & Parekh, A.D. (2014). *CFD analysis of energy separation of vortex tube employing different gases, turbulence models and discretisation schemes*, International Journal of Heat and Mass Transfer, 78, 360–370.
19. Thakare, H.R., & Parekh, A.D. (2017). *Experimental investigation & CFD analysis of Ranque–Hilsch vortex tube*, Energy, 133, 284–298.
20. Hooper, F.C., & Ambrose, C.W. (1973). An improved expansion process for the vapour refrigeration cycle, Proc. 4th Canadian Congr. Applied Mechanics, Montreal, 811–812.
21. Collins, R.L., & Lovelace, R.B. (1979). *Experimental study of two-phase propane expanded through the Ranque–Hilsch tube*, ASME Journal Heat Transfer, 101, 300–305. Vol
22. G.F., Nellis, S.,A., Klein, *The application of vortex tubes to refrigeration cycles. International refrigeration and air conditioning conference*, 2002, Purdue University, USA, Paper 537.
23. Sarkar, J. (2013). *Exergy analysis of vortex tube expansion vapor compression refrigeration system*, International Journal of Exergy, 13, 431–446.
24. Acar, S.M., & Arslan, O. (2017). *Exergo-economic evaluation of a new drying system boosted by Ranque–Hilsch vortex tube*, Applied Thermal Engineering, 124, 1–16.
25. S.M., Acar, *Thermodynamic evaluation and design of Ranque–Hilsch vortex tube aided hybrid cooling and drying system*, 2016, Dumlupinar University, Institute of Applied Sciences. Ph.D. Thesis, Kutahya, Turkey (in Turkish).
26. S., Bell, *A beginner's guide to uncertainty of measurement*, 1999, Measurement Good Practice Guide 11, Issue 2, Centre for Basic, Thermal and Length Metrology National Physical Laboratory, UK.
27. Doymaz, I. (2007). *Air-drying characteristics of tomatoes*, Journal of Food Engineering, 78, 1291–1297.

28. ASHRAE, *Handbook of Refrigeration*, 2010. Thermal properties of foods. ISBN 978-1-933742-82-3, American Society of Heating, Refrigerating and Air-Conditioning Engineers, Inc. 1791 Tullie Circle, N.E., Atlanta, GA 30329.
29. Ahrendts, J. (1980). *Reference states*, Energy, 5, 667–677.
30. Midilli, A., & Kucuk, H. (2003). *Energy and exergy analyses of solar drying process of pistachio*, Energy, 28, 539–556.
31. E. A., Yılmaz, *Price Proposal for Ranque–Hilsch Vortex Tube Supported Cooling System*, 2015, TESTTEKNIK.
32. CSB (T.C. Cevre ve Sehircilik Bakanlıgı), Ministry of Environment And Urbanization of Turkish Rebuplic, **http://www.csb.gov.tr**, Unit price of cooling unit used in system, [Last access: September 2015].
33. Guler, T., & Yucedag, M. (2011). *Feasibility report of atmosphere controlled cold storage facility*, Direct Business Support Program, Fırat Development Agency (in Turkish).
34. YogunluYuzeroglu, A., Hopoglu, M.S., & Gokce, S.G. (2013). *The analysis and pre-feasibility of frozen fruit and vegetable sector*, Fırat Development Agency (in Turkish).
35. **http://isotsatisi.com/kategori-6-KURU_KISLIKLAR.html**, The market price of dried tomatoes [Last access: September 2015] (in Turkish).
36. The market price of dried tomatoes, **http://www.organikim.com.tr/organik-domates-kurusu-200-gr** [Last access: September 2015] (in Turkish).
37. The market price of dried tomatoes, **http://tazekuru.com/urunler/64/kurutulmus-domates-100g-?gclid=-CLiLs-chMgCFSLnwgod-rgHiA** [Last access: September 2015] (in Turkish).
38. Anonym, (2015), Unit costs for cooling product, oral interviews with cold storage worker, Yalova, Turkey.
39. EMRA, (2015), *Energy Market Regulatory Authority board decision*, Decision No: 5666, Official Gazette of Turkish Republic No. 29401, June 29, 2015 (in Turkish).
40. The price of fresh tomatoes, **http://www.adana-bld.gov.tr/halfiyatlari.html** [Last access: September 2015] (in Turkish).
41. CBRT (Central Bank of Republic of Turkish), Interest rate, **http://www.tcmb.gov.tr/wps/wcm/connect/tcmb+tr/tcmb+tr/main+menu/duyurular/basin/2015/duy2015-13** [Last access: September 2015] (in Turkish).
42. CBRT (Central Bank of Republic of Turkish), Discount rate, **http://www.tcmb.gov.tr/wps/wcm/connect/tcmb+tr/tcmb+tr/main+menu/para+politikasi/reeskont+ve+avans+faiz+oranlari** [Last access: September 2015] (in Turkish).